

## Model for faceting in a kinetically controlled crystal growth

A. A. Golovin\* and S. H. Davis

*Department of Engineering Sciences and Applied Mathematics, Northwestern University, Evanston, Illinois 60208-3100*

A. A. Nepomnyashchy

*Department of Mathematics and Minerva Center for Nonlinear Physics of Complex Systems, Technion, Israel Institute of Technology, Haifa 32000, Israel*

(Received 4 August 1998)

A two-dimensional anisotropic nonlinear evolution equation is derived to model the formation of facets and corners in the course of kinetically controlled crystal growth. The equation is solved numerically in particular cases corresponding to the faceting of [001], [111], and [110] growing crystal surfaces, and the formation of hill-and-valley structures in the form of square, triangular, and rhombic pyramids; grooves are observed as well. The pyramidal slopes far from the vertices are found analytically, and in particular cases exact solutions of the equation are found. The pyramidal structures coarsen in time, and the rate of coarsening is studied. [S1063-651X(99)07401-2]

PACS number(s): 81.10.Aj, 81.30.Fb, 64.60.-i, 68.10.Cr

### I. INTRODUCTION

Anisotropic surface tension is one of the main causes of the formation of facets and corners during crystal growth [1–3]. If the surface-tension anisotropy is large, some orientations of the crystal surface are unstable and missing in the crystal equilibrium shape [4,5]. The decay of an unstable crystal surface into faces with stable orientations is analogous to spinodal decomposition [6,7,2,8–10]. In the case of the faceting transition caused, say, by a temperature change [11–13], the spinodal decomposition of a crystal surface can be described by phenomenological evolution equations for the order parameter — the local surface slope [7–9]. These equations are similar to the Cahn-Hilliard equation [14], which describes the dynamics of spinodal decomposition, and their solutions exhibit the formation of hill-and-valley structures of new crystal faces with stable orientations which correspond to bitangent points of the surface free energy. The structures coarsen in time with the rate depending on the mechanism of facet growth as well as on the effective dimension of the structure [15,8,9].

If the faceting occurs in the course of a crystal growth controlled by attachment kinetics, e.g., during the solidification in a hypercooled melt, the Cahn-Hilliard type evolution equation describing the formation of facets with stable orientations is modified by convective nonlinear terms [16,17] similar to those of the Burgers or Kuramoto-Sivashinsky equations (see also [18], where the Kuramoto-Sivashinsky equation, modified by the additional term typical of the Cahn-Hilliard equation, was derived for the evolution of steps on a crystal surface growing from the vapor in the presence of steps stiffness anisotropy). The effect of attachment kinetics destroys the bitangent construction and leads to a fast coarsening with time  $t$  at late stages; namely, it was found [17] that the mean spatial scale of quasi-one-

dimensional structure of grooves,  $L(t)$ , grows as  $L(t) \sim t^{1/2}$ . In this case the crystal faceting is analogous to the spinodal decomposition of driven systems [19,20].

In the present paper, the one-dimensional theory developed in [17] is extended and this is proposed as a phenomenological model for faceting of thermodynamically unstable two-dimensional surfaces of three-dimensional crystals in the course of kinetically controlled growth; for example when vapor deposition, gas or liquid phase epitaxial growth, etc., has the evaporation-condensation mechanism as dominant. A similar model is also derived for solidification of a hypercooled melt in order to study the effect of the coupling between the temperature field and the shape of the surface on the formation of hill-and-valley structure. Our theory serves as a generalization in the presence of the growth of phenomenological models proposed in [8,9] for the faceting of thermodynamically unstable crystal surfaces without net surface growth. It also extends a wide class of models of surface growth processes (see [21] for review) to the growth of thermodynamically unstable surfaces.

### II. PHENOMENOLOGICAL APPROACH

In this section an evolution equation is derived for the kinetically controlled growth of a thermodynamically unstable crystal surface with anisotropic surface tension using a phenomenological approach similar to that described in [21]. Consider a crystal growing from the other phase, which is referred to as a “liquid,” but which can be either a pure melt, or a solution, or a vapor. There are two modes of crystal growth: slow growth, such that there is a *local* thermodynamic equilibrium at the crystal-liquid interface and the growth is controlled by thermal or chemical diffusion in the liquid, and fast growth, controlled by the attachment kinetics, in which case there is no thermodynamic equilibrium at the crystal-liquid interface. The latter case will be addressed herein.

In equilibrium if the crystal surface is planar, chemical potentials of the liquid and the solid,  $\mu_l$  and  $\mu_s$ , respectively, are equal,  $\mu_l^e = \mu_s^e$ . For the curved surface, there is a jump of the equilibrium chemical potential at the interface

\*Present address: Department of Chemical Engineering, Technion, Israel Institute of Technology, Haifa 32000, Israel.

due to the solid-liquid surface tension. For a crystal with a surface given by  $z=h(x,y)$ , this jump is found from the condition [5]

$$\frac{\delta F}{\delta h} = 0, \quad (1)$$

where  $F$  is the total free energy of the crystal-liquid system. The free energy  $F$  is a sum of the bulk energies,  $F_s$  and  $F_l$ , of the crystal and the liquid, respectively, and the interfacial energy,  $F_i$ ,

$$F = F_l + F_s + F_i = \int \mu_s h(x,y) dx dy - \int \mu_l h(x,y) dx dy + \int \gamma \sqrt{1 + |\nabla h|^2} dx dy, \quad (2)$$

where  $\gamma$  is the surface tension and  $\nabla = (\partial_x, \partial_y)$ . If Eq. (2) is substituted into Eq. (1), one obtains

$$\mu_l^e - \mu_s^e = \mathcal{L}_h(I), \quad (3)$$

where  $I$  is the *weighed* surface tension,

$$I \equiv \gamma \sqrt{1 + |\nabla h|^2}, \quad (4)$$

and  $\mathcal{L}_h$  is the linear functional whose form depends on whether the surface tension is isotropic or not, and whether edges and corners are present on the crystal surface [22,17]. For isotropic surface tension,  $\gamma = \text{const}$ ,  $\mathcal{L}_h(I) = 2\gamma\mathcal{K}$ , where  $\mathcal{K}$  is the surface mean curvature.

Equation (3) gives the Gibbs-Thomson relation for the deviation of the equilibrium temperature at a curved liquid-crystal interface,  $T_e$ , from the equilibrium melting temperature at a planar interface,  $T_m$ . Namely, expanding  $\mu_{l,s}(T_e) \approx \mu_{l,s}(T_m) + (\partial\mu_{l,s}/\partial T)(T_e - T_m)$ , and using the thermodynamic relation  $\partial\mu_{l,s}/\partial T = -s_{l,s}$ , where  $s_{l,s}$  are the liquid and solid specific entropies, one gets

$$T_e = T_m \left[ 1 - \frac{\mathcal{L}_h(I)}{L_v} \right], \quad (5)$$

where  $L_v = T_m(s_l - s_s)$  is the latent heat per unit volume.

Consider the case of fast growth, i.e., when the growth occurs in the absence of thermodynamic equilibrium at the crystal-liquid interface. If there is no local thermodynamic equilibrium, the difference between the liquid and solid chemical potentials,  $\Delta = \mu_l - \mu_s$ , deviates from its equilibrium value,  $\Delta^e$ , prescribed by the liquid-crystal surface-tension,  $\Delta^e = \mu_l^e - \mu_s^e = \mathcal{L}_h(I)$ . For small deviations from the equilibrium,  $|(\Delta - \Delta^e)/\Delta^e| \ll 1$ , the local normal velocity,  $v_n$ , of the crystal surface growing into the liquid is proportional to the local deviation from the thermodynamic equilibrium, i.e.,

$$v_n = \kappa(\Delta - \Delta^e) = \kappa[\Delta - \mathcal{L}_h(I)], \quad (6)$$

where  $\kappa$  is the *kinetic coefficient* that generally depends on the local molecular structure of the crystal surface and can vary with the surface orientation. In this paper the anisotropy of  $\kappa$  is ignored and  $\kappa$  is assumed to be constant.

Consider the surface tension to be anisotropic, i.e., to be a function of the local surface orientation. Moreover, consider the case when some of the crystal surface orientations are thermodynamically unstable. This instability yields the formation of facets divided by edges and corners on the crystal surface. The regions of edges and corners are usually considered to have additional energies [8,9,16,23] which can be associated with the additional energy of interaction of steps on the crystal surface in the corner region where the gradient of the steps density is large [17]. This is equivalent to the dependence of the surface tension  $\gamma$  on the local curvature [17], and provides for a short-wave regularization of the faceting instability [17,16]. Thus, it is assumed that

$$\gamma = \gamma(h_x, h_y, h_{xx}, h_{xy}, h_{yy}). \quad (7)$$

This gives for  $\mathcal{L}_h(I)$

$$\begin{aligned} \mathcal{L}_h(I) = & -\frac{d}{dx} \frac{\partial I}{\partial h_x} - \frac{d}{dy} \frac{\partial I}{\partial h_y} + \frac{d^2}{dx^2} \frac{\partial I}{\partial h_{xx}} \\ & + \frac{d^2}{dx dy} \frac{\partial I}{\partial h_{xy}} + \frac{d^2}{dy^2} \frac{\partial I}{\partial h_{yy}}. \end{aligned} \quad (8)$$

The normal velocity of the growing surface is related to the surface shape as

$$v_n = \frac{h_t}{(1 + |\nabla h|^2)^{1/2}}. \quad (9)$$

The difference between the liquid and the crystal chemical potentials,  $\Delta$ , which is the *driving force* of the crystal growth, is a function of temperature and concentration, and it depends on the temperature and concentration fields around the crystal. The latter, in turn, are often determined by the crystal shape itself, and in this case  $\Delta$  depends on  $h$ .

Thus, using Eqs. (8), (9), (3), one obtains from Eq. (6) the following evolution equation for  $h(x,y,t)$ :

$$\frac{h_t}{(1 + |\nabla h|^2)^{1/2}} = \kappa[\Delta(h) + \mathcal{E}(h)], \quad (10)$$

where  $\mathcal{E}(h)$  is

$$\begin{aligned} \mathcal{E}(h) = & \frac{\partial^2 I}{\partial (h_x)^2} h_{xx} + 2 \frac{\partial^2 I}{\partial h_x \partial h_y} h_{xy} + \frac{\partial^2 I}{\partial (h_y)^2} h_{yy} - \frac{\partial^2 I}{\partial (h_{xx})^2} h_{xxx} - 2 \frac{\partial^2 I}{\partial h_{xy} \partial h_{xx}} h_{xxy} - \left( \frac{\partial^2 I}{\partial (h_{xy})^2} + 2 \frac{\partial^2 I}{\partial h_{xx} \partial h_{yy}} \right) h_{xxyy} \\ & - 2 \frac{\partial^2 I}{\partial h_{xy} \partial h_{yy}} h_{xyyy} - \frac{\partial^2 I}{\partial (h_{yy})^2} h_{yyyy}. \end{aligned} \quad (11)$$

There are three cases for the dependence  $\Delta(h)$ . In the simplest case, if one can neglect the effect of the variation of the temperature or concentration field with the crystal shape on the difference between the liquid and crystal chemical potentials, one can simply set  $\Delta(h) = \text{const}$ . If the variation of temperature or concentration field is important and occurs near the crystal surface in a boundary layer whose thickness is small in comparison with the surface radius of curvature, the dependence  $\Delta(h)$  is *local*, and is generally represented as a nonlinear differential operator. If the characteristic scale of the temperature or concentration field is comparable with the radius of curvature of the crystal surface, then the dependence  $\Delta(h)$  is *nonlocal*, and is usually expressed as a nonlinear integro-differential operator. Below the first two cases are examined.

### III. CONSTANT DRIVING FORCE

The simplest case is when  $\Delta(h) = \Delta_0 = \text{const}$ . Consider a crystal with the lattice having a cubic symmetry. The crystal surface tension has a cubic anisotropy, and its dependence on the surface curvature [17] is also taken into account. Thus, following [24], we suggest that in the frame of reference  $\{\mathbf{e}_x^0, \mathbf{e}_y^0, \mathbf{e}_z^0\}$  aligned with the principal crystal directions ( $[100], [010], [001]$ ),

$$\gamma = \gamma_0 \left[ 1 + \epsilon_4 (n_x^4 + n_y^4 + n_z^4) + \epsilon_6 (n_x^6 + n_y^6 + n_z^6) + \dots \right] + \frac{\delta}{2} \mathcal{K}^2, \quad (12)$$

where  $n_x, n_y, n_z$  are the coordinates of the local unit normal to the crystal surface that can be expressed in terms of the angular spherical coordinates  $\theta$  and  $\phi$  as  $n_x = \sin \theta \cos \phi$ ,  $n_y = \sin \theta \sin \phi$ ,  $n_z = \cos \theta$ ,  $\gamma_0$  is a constant characterizing mean surface tension of the crystal,  $\epsilon_4, \epsilon_6, \dots$  are the coefficients of the surface-tension anisotropy, and  $\delta = \text{const} > 0$ . Consider a planar crystal surface growing with the orientation characterized by a normal vector  $\mathbf{e}_z = (\sin \theta \cos \phi, \sin \theta \sin \phi, \cos \theta)$  and choose the other two basis vectors in the surface plane to be  $\mathbf{e}_x = \mathbf{e}_z \times \mathbf{e}_z^0 / |\mathbf{e}_z \times \mathbf{e}_z^0|$ ,  $\mathbf{e}_y = \mathbf{e}_z \times \mathbf{e}_x / |\mathbf{e}_z \times \mathbf{e}_x|$ . In the coordinate system  $\{\mathbf{e}_x, \mathbf{e}_y, \mathbf{e}_z\}$  the position of the crystal surface is given by  $z = h(x, y, t)$ . The weighed surface tension  $I$  defined by Eq. (4) can be expanded for  $|h_x| \ll 1$ ,  $|h_y| \ll 1$  as

$$\begin{aligned} I(h_x, h_y, h_{xx}, h_{xy}, h_{yy}) \\ = \gamma_0 \sum_{m,n=0}^{\infty} e_{mn}(\epsilon_4, \epsilon_6, \theta, \phi) h_x^m h_y^n \\ + \frac{\delta}{2} (h_{xx}^2 + 2h_{xx}h_{yy} + h_{yy}^2) + \dots \end{aligned} \quad (13)$$

Here the coefficients  $e_{ij}$  are the functions of the direction of the crystal growth and of the anisotropy coefficients which are computed in [25] and reproduced in the Appendix; the dots denote higher-order terms.

After the transformation  $t \rightarrow t/(\kappa \Delta_0)$ , Eq. (10) reads

$$h_t = \sqrt{1 + |\nabla h|^2} [1 + \Gamma \mathcal{E}(h)], \quad (14)$$

where  $\Gamma = \gamma_0 / \Delta_0$ .

Equation (14) has a solution corresponding to a planar uniformly growing surface (uniformly propagating crystallization front)  $h = t$  (the dimensional velocity of the front is  $\kappa \Delta_0$ ). Transform to the frame moving with the planar front, change the variable  $h \rightarrow h + t$ , and expand Eq. (14) for  $|h_t| \ll 1$ ,  $|\nabla h| \ll 1$ . Keeping the terms up to the second order, one obtains

$$h_t - \frac{1}{2} (\nabla h)^2 - \Gamma \mathcal{E}_2(h) = 0, \quad (15)$$

where  $\mathcal{E}_2$  is the linear differential operator

$$\mathcal{E}_2 = \nabla A \nabla^\top, \quad A = \begin{pmatrix} 2e_{20} & e_{11} \\ e_{11} & 2e_{02} \end{pmatrix}. \quad (16)$$

Equation (15) is an anisotropic Burgers equation. It can also be called the anisotropic, deterministic Kardar-Parisi-Zhang (AKPZ) equation [26,27]. With noise added, this equation describes kinetic roughening of vicinal surfaces [26], epitaxial growth, etc. (see [21] for review). If the eigenvalues of the anisotropy matrix  $A$  are positive, Eq. (15) describes hill-and-valley structure propagating along the interface with the amplitude determined by initial conditions [28]. In this case the anisotropic surface tension prevents the formation of sharp corners in the course of kinetically controlled crystal growth [29,30].

When at least one of the eigenvalues of  $A$  is negative, the crystal surface with the orientation characterized by the anisotropy matrix  $A$  is *thermodynamically unstable*. As discussed above, this instability yields formation of facets and corners. However, in this case Eq. (15) is ill-posed since it does not have a short-wave cutoff. In order to describe the dynamics of the formation of facets and corners, one has to keep higher-order terms in the evolution equation for the crystal surface.

Keeping the terms up to the fourth order in Eq. (14), one obtains for the shape of the crystal surface in the moving frame the following evolution equation:

$$\begin{aligned} h_t = \frac{1}{2} (\nabla h)^2 - \frac{1}{8} (\nabla h)^4 + \Gamma \left( 1 + \frac{1}{2} (\nabla h)^2 \right) \mathcal{E}_2(h) + \Gamma \mathcal{E}_3(h) \\ + \Gamma \mathcal{E}_4(h) + O(|\nabla h|^6), \end{aligned} \quad (17)$$

where one gets from Eqs. (11) and (13),

$$\begin{aligned} \mathcal{E}_2(h) &= \alpha_{ij} h_{x_i x_j}, \\ \mathcal{E}_3(h) &= \beta_{ijk} h_{x_i x_j} h_{x_k}, \end{aligned} \quad (18)$$

$$\mathcal{E}_4(h) = \gamma_{ijkl} h_{x_i x_j} h_{x_k} h_{x_l} - \delta_{ijkl} h_{x_i x_j x_k x_l},$$

and  $i, j, k = 1, 2$ ,  $x_1 = x$ ,  $x_2 = y$ ,  $\alpha_{ij}$ ,  $\beta_{ijk}$ ,  $\gamma_{ijkl}$ , and  $\delta_{ijkl}$  do not change with the permutations of their indices;

$$\begin{aligned}
\alpha_{11} &= 2e_{20}, \quad \alpha_{12} = e_{11}, \quad \alpha_{22} = 2e_{02}, \\
\beta_{111} &= 6e_{30}, \quad \beta_{112} = 2e_{21}, \quad \beta_{221} = 2e_{12}, \quad \beta_{222} = 6e_{03}, \\
\gamma_{1111} &= 12e_{40}, \quad \gamma_{1112} = 3e_{31}, \quad \gamma_{1122} = 2e_{22}, \quad \gamma_{1222} = 3e_{13}, \quad \gamma_{2222} = 12e_{04}, \\
\delta_{1111} &= \delta_{2222} = 3\delta_{1122} = \delta/\gamma_0, \quad \delta_{1112} = \delta_{1222} = 0.
\end{aligned} \tag{19}$$

The summation over repeated indices is assumed.

The nonlinear terms  $(\nabla h)^2/2 - (\nabla h)^4/8$  on the right-hand side of Eq. (17) stem from the projection of the local normal velocity of the crystallization front on the  $z$  axis [cf. Eq. (9)]. Usually, only a  $(\nabla h)^2$  term is present in this type of equation since it already describes the kinematic effect of the interfacial slope [21]. Moreover, although the two-term expansion that includes also the  $(\nabla h)^4$  term is more accurate for small surface slopes, it can lead to artifacts if the slope of the interface is large. Therefore, the fourth-order kinematic term in the evolution equation is omitted. Thus, Eq. (17) is written in the following form:

$$\begin{aligned}
h_t &= \frac{1}{2} |\nabla h|^2 + h_{xx} [\mu_{11} + \kappa_{11} h_x + \lambda_{11} h_y + a_{11} h_x^2 + b_{11} h_y^2 + c_{11} h_x h_y] + h_{xy} [\mu_{12} + \kappa_{12} h_x + \lambda_{12} h_y + a_{12} h_x^2 + b_{12} h_y^2 + c_{12} h_x h_y] \\
&+ h_{yy} [\mu_{22} + \kappa_{22} h_x + \lambda_{22} h_y + a_{22} h_x^2 + b_{22} h_y^2 + c_{22} h_x h_y] - \nu \nabla^4 h,
\end{aligned} \tag{20}$$

where

$$\begin{aligned}
\mu_{11} &= 2\Gamma e_{20}, \quad \mu_{12} = 2\Gamma e_{11}, \quad \mu_{22} = 2\Gamma e_{02}, \\
\kappa_{11} &= 6\Gamma e_{30}, \quad \kappa_{12} = 4\Gamma e_{21}, \quad \kappa_{22} = 2\Gamma e_{12}, \\
\lambda_{11} &= 2\Gamma e_{21}, \quad \lambda_{12} = 4\Gamma e_{12}, \quad \lambda_{22} = 6\Gamma e_{03}, \\
a_{11} &= \Gamma(12e_{40} + e_{20}), \quad a_{12} = \Gamma(6e_{31} + e_{11}), \\
a_{22} &= \Gamma(2e_{22} + e_{02}), \\
b_{11} &= \Gamma(2e_{22} + e_{20}), \quad b_{12} = \Gamma(6e_{13} + e_{11}), \\
b_{22} &= \Gamma(12e_{04} + e_{02}), \\
c_{11} &= 6\Gamma e_{31}, \quad c_{12} = 8\Gamma e_{22}, \quad c_{22} = 6\Gamma e_{13}, \\
\nu &= \delta/\Delta_0.
\end{aligned} \tag{21}$$

Equation (20) is related to those derived in [8,9] for the faceting of crystal surfaces with unstable orientations when there is no surface growth. The coefficients  $\mu_{ij}$  characterize the linear faceting instability of the thermodynamically unstable surface, and the coefficients of the nonlinear terms determine the stable orientations of the appearing facets and the symmetry of the faceted structure. The linear damping coefficient  $\nu$  characterizes the stabilizing effect of the additional energy of edges and determines their widths (see below). The new feature is that Eq. (20) describes the faceting instability in the course of kinetically controlled crystal growth, which accounts for the presence of the ‘‘convective’’ term  $\frac{1}{2}(\nabla h)^2$ . On the other hand, it can be considered as a generalization of isotropic growth models reviewed in [21] for the case of an evaporation-condensation growth mechanism. Other mechanisms of anisotropic growth of *thermodynamically stable* surfaces, such as anisotropic kinetics and anisotropic step flow, were considered in [26,31]. Equation (20) is now considered here to be a phenomeno-

logical model for the formation of facets and corners in the kinetically controlled growth of a *thermodynamically unstable* surface, in the simplest case of a constant driving force.

In the next section a similar evolution equation is derived for a more complicated case, when the difference between the crystal and liquid chemical potentials is not constant, but it is locally coupled to the temperature field in a thermal diffusion boundary layer near the crystal surface. As an example, the solidification of a hypercooled melt is discussed.

#### IV. SOLIDIFICATION IN A HYPERCOOLED MELT: EFFECT OF THERMAL DIFFUSION BOUNDARY LAYER

Consider a solidification front rapidly propagating through a hypercooled melt, so that the rate of solidification is controlled by the attachment kinetics. In this case the local velocity,  $v_n$ , of the crystal growth in the direction normal to the surface at a given point is given by Eq. (6). The temperature at the interface,  $T_i$ , is less than the equilibrium temperature,  $T_e$ , given by Eq. (5). Taking into account the temperature dependence of the chemical potentials and expanding  $\mu_{l,s}(T_i) \approx \mu_{l,s}(T_m) + (\partial\mu_{l,s}/\partial T)(T_i - T_m)$ , one obtains from Eq. (6)

$$v_n = \bar{\kappa}(T_e - T_i), \tag{22}$$

where  $\bar{\kappa} = \kappa L_v/T_m$  is the renormalized kinetic coefficient which is assumed to be constant. Note that Eq. (22) is valid for small deviations from the equilibrium. This is not the case for a hypercooled melt and a nonlinear dependence of the normal velocity on temperature likely applies [32]. However, for our purpose, in order to show the effect of the temperature field on the formation of facets in the course of kinetically controlled growth of a thermodynamically unstable crystal surface, it is sufficient to use Eq. (22) as an approximation.

Choose the following scalings:  $\chi_T/(\bar{\kappa}\Delta T)$  as the unit length,  $\chi_T/(\bar{\kappa}\Delta T)^2$  as the unit time, where  $\Delta T = T_m - T_\infty$  is the difference between the melting temperature at the planar

front growing in the given direction,  $T_m$ , and the temperature at infinity  $T_\infty$ , and  $\chi_T$  is the thermal diffusivity of the melt.

Consider a plane solidification front moving with (as yet unknown) velocity  $V$ . The shape of the deformed front in the frame of reference moving with the velocity  $V$  is described by  $z=h(x,y,t)$ , where  $z$  is the coordinate in the propagation direction of the planar front, and  $x$  and  $y$  are the coordinates along the planar front. In the frame of reference moving with the front [ $x$ ,  $y$ ,  $\zeta=z-Vt-h(x,y,t)$ ], the kinetically controlled solidification process is described by the following system of dimensionless equations and boundary conditions (the same notation is used for the dimensional and dimensionless coordinates) [33]:

$$\begin{aligned} \Phi_t &= [1 + (\nabla h)^2] \Phi_{\zeta\zeta} + \nabla^2 \Phi + (V + h_t - \nabla^2 h) \Phi_\zeta \\ &\quad - 2 \nabla h \cdot \nabla \Phi_\zeta, \\ z = \infty, \quad \Phi &= 0; \end{aligned} \quad (23)$$

$$z = 0, \quad S(V + h_t) = -\Phi_\zeta + \nabla h \cdot (\nabla \Phi - \Phi_\zeta \nabla h), \quad (24)$$

$$\frac{V + h_t}{[1 + (\nabla h)^2]^{1/2}} = 1 - \Phi + \Gamma \mathcal{E}(h), \quad (25)$$

where  $\Phi = (T - T_\infty)/\Delta T$  is the dimensionless temperature,  $S = L_v/(\rho c_p \Delta T)$  is the Stefan number,  $\Gamma = \gamma_0 \bar{\kappa} T_m/(\chi_T L)$ , and  $\rho$  and  $c_p$  are the density and the specific heat, which are assumed to be equal for both crystal and melt. Equation (23) describes heat transport in the liquid phase, the boundary condition (24) represents the balance of energy at the solidification front, and the boundary condition (25) describes the kinetically controlled growth (22) with the equilibrium temperature governed by the anisotropic Gibbs-Thomson effect (5). In the problem (23)–(25) heat transfer is neglected in the solid phase (a *one-side model*). The additional energy consumed in the phase transformation due to the creation of a new interface in the growth of a crystal with curved surface [34,35] is also neglected.

Assume that the thickness of the thermal diffusion boundary layer is much smaller than the radius of curvature of the crystal surface. Thus consider perturbations of the crystallization front to be long wave, and apply a long-scale expansion to the problem (23)–(25) suggesting  $|h_x|, |h_y| \ll 1$ . Thus, introduce the long-scale coordinates  $(X, Y) = \epsilon(x, y)$ ,  $\epsilon \ll 1$ , the hierarchy of slow times  $T_2, T_3, T_4, \dots$  such that  $T_k = \epsilon^k t$ ,  $k = 2, 3, \dots$ , and consider  $h(X, Y, T_2, T_3, T_4, \dots) = O(1)$ ,  $\Phi(\zeta, X, Y, T_2, T_3, T_4, \dots) = \Phi^{(0)}(\zeta, X, Y, T_2, T_3, T_4, \dots) + \epsilon^2 \Phi^{(2)}(\zeta, X, Y, T_2, T_3, T_4, \dots) + \epsilon^3 \Phi^{(3)}(\zeta, X, Y, T_2, T_3, T_4, \dots) + \epsilon^4 \Phi^{(4)}(\zeta, X, Y, T_2, T_3, T_4, \dots) + \dots$ ; functions  $\Phi^{(i)}$  must decay at infinity.

In the order  $O(1)$  one obtains the following solution [33]:

$$\Phi^{(0)} = S \exp(-V\zeta), \quad V = 1 - S, \quad (26)$$

which corresponds to a planar crystallization front propagating with the velocity  $V$  which is a function of the undercooling  $S^{-1}$ . Solution (23) exists only at  $S < 1$ , i.e., if the undercooling  $\Delta T > L_v/(\rho c_p)$  (the *hypercooled melt*).

From the solvability condition of the problem in the order  $O(\epsilon^2)$  one obtains the following evolution equation for  $h$ :

$$h_{T_2} - \frac{V}{2} |\nabla h|^2 - \mathcal{E}_2^s(h) = 0, \quad (27)$$

where  $\mathcal{E}_2^s$  is the linear differential operator

$$\mathcal{E}_2^s = -\frac{S}{V} \nabla^2 + \Gamma \nabla A \nabla^\top, \quad (28)$$

where the anisotropy matrix  $A$  is defined in Eq. (16) and  $\nabla$  acts on the long-scale coordinates.

Equation (27) differs from Eq. (15) by the Laplacian in the operator  $\mathcal{E}_2^s$  that describes the effect of the thermal field in the diffusion boundary layer. It can be seen that even if the eigenvalues of the anisotropy matrix  $A$  are positive and the crystal surface is thermodynamically stable, it can become *morphologically unstable* for  $1 > S > S_{\text{cr}}$ , where  $S_{\text{cr}}$  depends on the anisotropic surface tension [25].

As a solvability condition in the order  $O(\epsilon^3)$ , one gets the equation

$$h_{T_3} = \Gamma \mathcal{E}_3(h), \quad (29)$$

where  $\mathcal{E}_3(h)$  is defined by Eqs. (18) and (19).

However, solutions of Eq. (29) blow up, and in order to obtain the equation describing the long-time evolution of the crystal surface, one must proceed to the fourth order,  $O(\epsilon^4)$ , the solvability condition for which gives

$$\begin{aligned} h_{T_4} &= \mathcal{S}_4(h) - \frac{2S}{V^3} \frac{\partial(h_x, h_y)}{\partial(X, Y)} + \frac{S}{2V} \nabla h \cdot \nabla(\nabla h)^2 - \frac{V}{8} (\nabla h)^4 \\ &\quad + \mathcal{N}_4(h), \end{aligned} \quad (30)$$

where

$$\mathcal{S}_4 = -\frac{S(V+1)}{V^5} \nabla^4 - \frac{S(V+2)}{V^4} \Gamma \nabla^2 \mathcal{E}_2 - \frac{S}{V^3} \Gamma^2 \mathcal{E}_2^2, \quad (31)$$

$$\begin{aligned} \mathcal{N}_4(h) &= \Gamma \mathcal{E}_2(h) \left( \frac{S}{V^2} \nabla^2 h + \frac{1}{2} (\nabla h)^2 \right) \\ &\quad + \frac{S}{V^2} \Gamma \left( \nabla h \cdot \mathcal{E}_2(\nabla h) - \frac{1}{2} \mathcal{E}_2((\nabla h)^2) \right) + \Gamma \mathcal{E}_4(h), \end{aligned}$$

with  $\mathcal{E}_2$  and  $\mathcal{E}_4$  defined by formulas (16), (18), and (19).

Finally, going back to the initial variables  $x, y, t$ , one can unify Eqs. (15), (29), and (30) in a single evolution equation

$$\begin{aligned}
h_t - \frac{V}{2}(\nabla h)^2 = & h_{xx}[\mu_{11}^s + \kappa_{11}h_x + \lambda_{11}h_y + a_{11}^sh_x^2 + b_{11}h_y^2 + c_{11}h_xh_y] + h_{xy}[\mu_{12} + \kappa_{12}h_x + \lambda_{12}h_y + a_{12}h_x^2 + b_{12}h_y^2 + c_{12}^sh_xh_y] \\
& + h_{yy}[\mu_{22}^s + \kappa_{22}h_x + \lambda_{22}h_y + a_{22}h_x^2 + b_{22}^sh_y^2 + c_{22}h_xh_y] + g \frac{\partial(h_x, h_y)}{\partial(x, y)} - \chi_{ijkl}h_{x_i x_j x_k x_l}, \tag{32}
\end{aligned}$$

where

$$\begin{aligned}
\mu_{11}^s = & -\frac{S}{V} + \mu_{11}, \quad \mu_{22}^s = -\frac{S}{V} + \mu_{22}, \quad a_{11}^s = \frac{S}{V} + a_{11}, \quad b_{22}^s = \frac{S}{V} + b_{22}, \quad c_{12}^s = \frac{2S}{V} + c_{12}, \\
\chi_{1111} = & \frac{S(V+1)}{V^5} + \nu - \frac{2S(V+2)}{V^4}\Gamma e_{20} + \frac{4S}{V^3}\Gamma^2 e_{20}^2, \\
\chi_{1112} = & -\frac{S(V+2)}{2V^4}\Gamma e_{11} + \frac{2S}{V^3}\Gamma^2 e_{20}e_{11}, \\
\chi_{1122} = & \frac{S(V+1)}{3V^5} + \frac{\nu}{3} - \frac{S(V+2)}{3V^4}\Gamma(e_{20} + e_{02}) + \frac{4S}{3V^3}\Gamma^2 e_{20}e_{02}, \tag{33} \\
\chi_{1222} = & -\frac{S(V+2)}{2V^4}\Gamma e_{11} + \frac{2S}{V^3}\Gamma^2 e_{02}e_{11}, \\
\chi_{2222} = & \frac{S(V+1)}{V^5} + \nu - \frac{2S(V+2)}{V^4}\Gamma e_{02} + \frac{4S}{V^3}\Gamma^2 e_{02}^2, \\
g = & \frac{2S}{V^2}\left(\Gamma(e_{20} + e_{02}) - \frac{1}{V}\right),
\end{aligned}$$

the other coefficients are defined by Eq. (21), and, as in Eq. (20), the term with  $(\nabla h)^4$  in the expansion of the normal velocity of the crystallization front is omitted.

Equation (32) is asymptotically correct if  $\mu_{ij} = O(\epsilon^2)$  and  $\kappa_{ij}, \lambda_{ij} = O(\epsilon)$ . Otherwise, Eq. (32) should be considered as a model equation for describing formation of corners and facets caused by anisotropic surface tension in the course of kinetically controlled crystal growth when the effect of the thermal boundary layer near the crystal surface is important. One can see that the coefficients of Eq. (32) are determined not only by the anisotropy of the crystal surface tension, but also by the temperature field near the crystal surface, i.e., they depend also on the undercooling  $S^{-1}$ .

Equation (32) contains also a new term,  $g \partial(h_x, h_y)/\partial(x, y)$ , which is the main part of the Gaussian curvature,  $\mathcal{G} = (h_{xx}h_{yy} - h_{xy}^2)/(1 + |\nabla h|^2)^2$ , in the long-wave approximation. This term was first seen in [36] as part of the intrinsic equation of interfacial motion for solidification in a hypercooled melt in the case of isotropic surface tension; in the isotropic case the coefficient  $g$  coincides with the corresponding coefficient derived in [36]. Note that the evolution equation derived in [36] contains also a nonlinear term proportional to the square of the surface curvature,  $\mathcal{K}^2$ , which arises if one takes into account thermal diffusion in the crystal (the two-sided model). In the one-dimensional case the term with the Gaussian curvature disappears and Eq. (32) is reduced to the evolution equation derived in [17].

On the one hand, physical effects that would lead to the appearance of the term with the Gaussian curvature in the equation describing the evolution of the crystal surface are not clear. On the other hand, the Gaussian curvature is the surface invariant of the next order after the mean surface curvature, and one might expect it to appear naturally in the expansion with respect to small surface slopes. Below it is shown that the presence of this term leads, within the framework of the present model, to the formation of some of the patterns observed in crystal-growth experiments.

## V. FACETING OF GROWING SURFACES WITH DIFFERENT ORIENTATIONS WITH CONSTANT DRIVING FORCE

In this section consider the faceting of kinetically growing crystal surfaces with different orientations when the effects of the temperature variations in the diffusion boundary layer can be neglected (constant driving force). In this case the evolution of the shape of the crystal surface is described by Eq. (20). Equation (20) is solved numerically for different cases corresponding to different orientations of the growing crystal surface. A pseudospectral method is used with 128 modes in both directions and periodic boundary conditions, starting from small-amplitude random initial data. Time in-

tegration is performed in the Fourier space by means of the semi-implicit Adams-Bashforth/Crank-Nicolson scheme.

### A. Orientation [001]

For the growth of the [001] surface, the anisotropy coefficients are computed to be

$$\begin{aligned} e_{20} = e_{02} &= \frac{1}{2} - \frac{3}{2} \epsilon_4 - \frac{5}{2} \epsilon_6, \\ e_{40} = e_{04} &= -\frac{1}{8} + \frac{23}{8} \epsilon_4 + \frac{35}{8} \epsilon_6, \\ e_{22} &= -\frac{1}{4} + \frac{15}{4} \epsilon_4 + \frac{35}{4} \epsilon_6, \\ e_{11} = e_{30} = e_{21} = e_{12} = e_{03} = e_{31} = e_{13} &= 0. \end{aligned} \quad (34)$$

Equation (20) then reads

$$\begin{aligned} h_t &= -m \nabla^2 h - \nu \nabla^4 h + \frac{1}{2} (\nabla h)^2 + h_{xx} [a h_x^2 + b h_y^2] \\ &+ h_{yy} [b h_x^2 + a h_y^2] + c h_{xy} h_x h_y, \end{aligned} \quad (35)$$

where

$$\begin{aligned} m &= \Gamma(3\epsilon_4 + 5\epsilon_6 - 1), \quad a = \Gamma(33\epsilon_4 + 50\epsilon_6 - 1), \\ b &= \Gamma(6\epsilon_4 + 15\epsilon_6), \quad c = \Gamma(30\epsilon_4 + 70\epsilon_6 - 2), \end{aligned} \quad (36)$$

and  $\nu > 0$  is defined in Eq. (21). Consider the anisotropy coefficients  $\epsilon_4, \epsilon_6$  to be such that  $m > 0$ , so that the [001] surface is thermodynamically unstable and faceting occurs. The coefficients  $a$ ,  $b$ , and  $c$  characterizing the stable orientation of facets are taken to be positive, and the coefficient  $\nu$  is taken to be small in order to get sharp corners. Equation (35) does not have a rotational symmetry, but it is symmetric with respect to the transformations  $x \rightarrow -x$ ,  $y \rightarrow -y$ ,  $x \rightarrow y$ . This corresponds to the fourfold symmetry of the [001] crystal surface.

Figure 1 shows the results of the numerical solution of Eq. (35) for  $b/a \ll 1$ , i.e., for large anisotropy. Figures 1(a), 1(c), 1(e), and 1(g) exhibit the shape of the crystal surface at different times, and Figs. 1(b), 1(d), 1(f), and 1(h) show the corresponding surface contour plots. First one observes the formation of a hill-and-valley structure in the form of square pyramids. Note that the square shape of the pyramids can be distorted by their interaction. Such pyramids are often seen on the [001] surfaces growing by chemical vapor deposition [37], liquid phase epitaxy [38], molecular-beam epitaxy [39,40], etc. The pyramids with a characteristic horizontal scale  $\lambda_*$  corresponding to the most rapidly growing mode given by the linear stability analysis,  $\lambda_* = 2\pi\sqrt{2\nu/m}$ , are formed in a characteristic time,  $\tau_* = m^2/(4\nu)$ , and they have a characteristic *slope*. This slope is determined by the anisotropy of the surface energy as well as by the driving force of the crystal growth, i.e., the surface growth speed; the curvatures of the pyramid edges and vertex are determined by their additional energy (see below). After the pyramids have been formed, their slopes do not change any longer, but the struc-

ture coarsens in time forming square pyramids with larger horizontal spatial scale. Figure 2 shows the spatial distribution of the slopes of the pyramids,  $|\nabla h|$ , for two different times; one can see that the slopes remain unchanged during the coarsening process. This is a typical behavior of faceting instability of thermodynamically unstable surfaces, when the resulting slopes are determined by anisotropic surface free energy; in the one-dimensional case the slope of the facets is determined by the well-known double-tangent construction [1,8,9]. In the case of a kinetically controlled growth, when the evolution equation for the surface shape contains the nonlinear growth term  $|\nabla h|^2$ , the double-tangent construction is destroyed, but the slope of facets is still fixed and depends on both anisotropic surface free energy and the growth rate [17].

In our case the shapes of the pyramids far from the vertex and their final slopes can be found analytically. Consider a square pyramid oriented in such a way that the projections of its edges on the basis plane coincide with  $x$  and  $y$  axes. In this case, the pyramidal shape  $h(x, y, t)$  has the following asymptotics:

$$h \sim Ay + f(x) + \nu t \quad \text{as } y \rightarrow -\infty, \quad (37)$$

where  $\nu$  is the speed of the surface growth in the  $z$  direction (i.e., the nonlinear correction of the unit speed of planar surface growth in the laboratory frame),  $A$  is the slope of the pyramidal edges, and  $f(x)$  is a function to be determined. For  $x \rightarrow -\infty$  one has  $h \sim Ax + f(y) + \nu t$ . The function  $f$  must satisfy the compatibility condition

$$f'(\pm\infty) = \mp A \quad (38)$$

(the prime denotes differentiation).

By substituting Eq. (37) into Eq. (35), one obtains the following equation for  $f(x)$ :

$$\left(\frac{1}{2}A^2 - \nu\right) + \frac{1}{2}(f')^2 - (m - bA^2)f'' + a(f')^2 f'' - \nu f''' = 0. \quad (39)$$

Taking an ansatz [19]

$$f' = Q \tanh kx, \quad (40)$$

one obtains from Eq. (39)

$$Q^2 = \frac{3(m - bA^2)}{a} + \frac{3}{2a} \sqrt{\frac{6\nu}{a}} \operatorname{sgn} Q, \quad k = \sqrt{\frac{a}{6\nu}} |Q|, \quad (41)$$

where negative  $Q$  corresponds to a pyramid (hill) and positive  $Q$  corresponds to an antipyramid (hole), respectively;  $k$  is positive by definition. Equation (41) shows that the radius of curvature of the pyramidal edges  $\sim \sqrt{\delta/\gamma_0}$ , i.e., determined by their additional energy. From the compatibility condition,  $Q^2 = A^2$ , one finds the slope of the square pyramid edge far from the vertex,

$$A^\pm = \pm \sqrt{\frac{m \mp \sqrt{3\nu/(2a)}}{b + a/3}}, \quad (42)$$

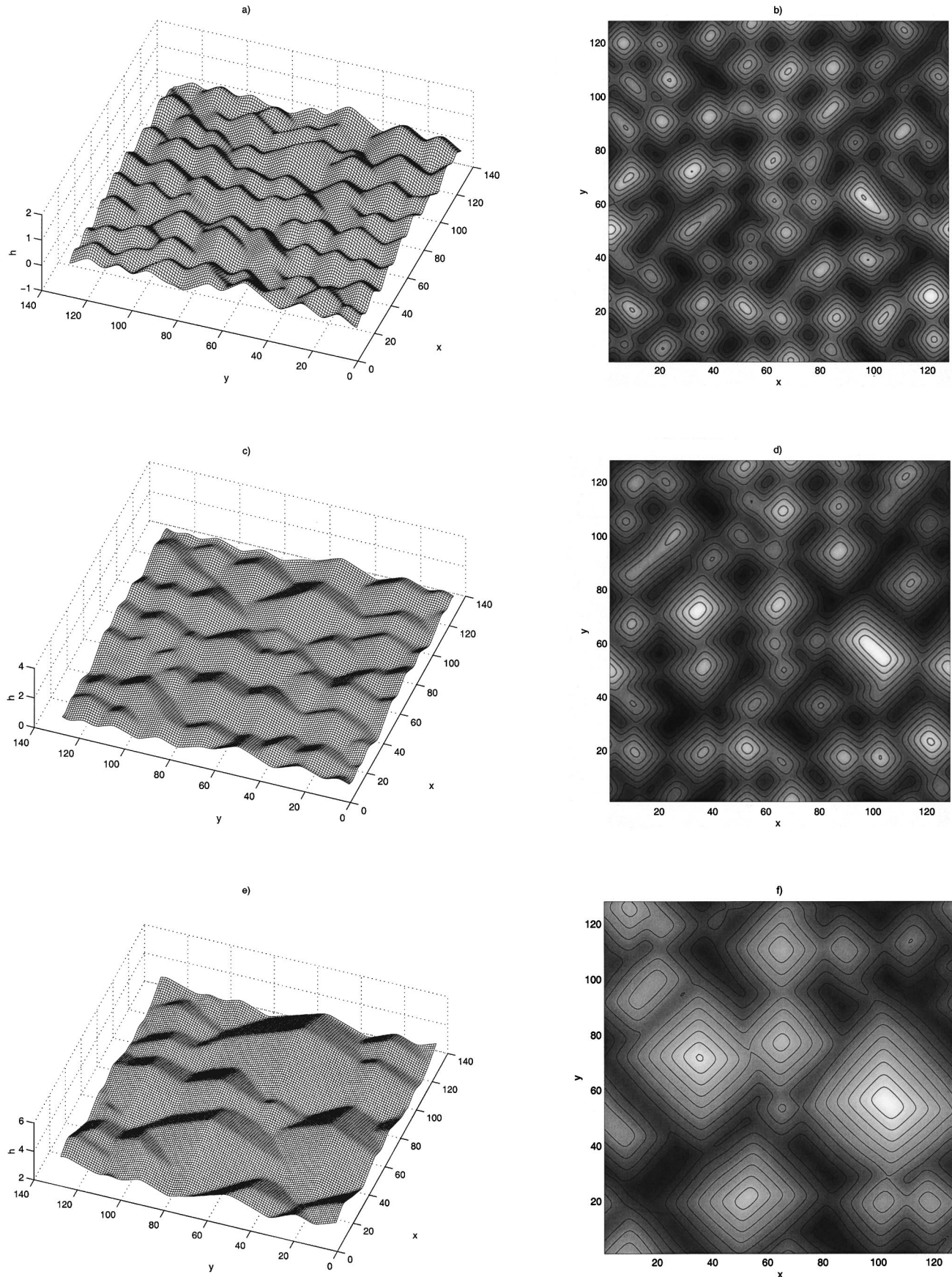


FIG. 1. Hill-and-valley structure on a growing crystal surface in the form of square pyramids: numerical solution of Eq. (35) at different moments of time: (a) and (b),  $t=10^4$ ; (c) and (d)  $t=2 \times 10^4$ ; (e) and (f)  $t=5 \times 10^4$ ; (g) and (h)  $t=10^5$ ;  $m=0.5$ ,  $\nu=0.001$ ,  $a=1.0$ ,  $b=0.1$ ,  $c=0.3$ . The spatial scale is arbitrary.

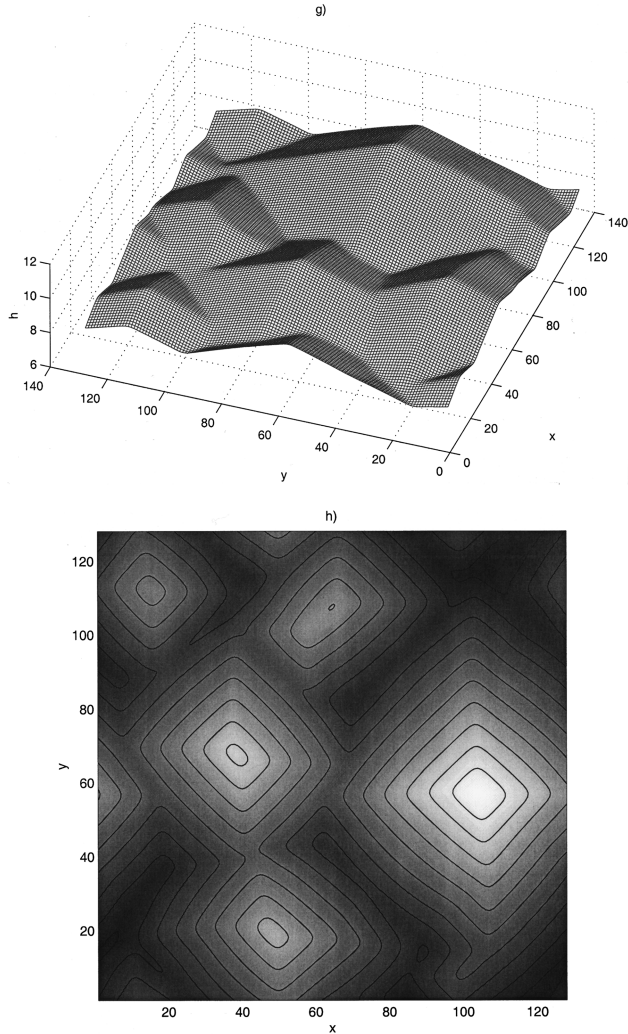


FIG. 1 (Continued).

where  $A^+$  corresponds to hills and  $A^-$  corresponds to holes. Thus, the shape of a square pyramid ( $h^+$ ) or antipyramid ( $h^-$ ) far from the vertex, for  $y \rightarrow -\infty$ , is

$$h^\pm(x, y, t) \sim A^\pm y \mp \sqrt{\frac{6\nu}{a}} \ln \left[ \cosh \left( \sqrt{\frac{a}{6\nu}} |A^\pm| x \right) \right] + (A^\pm)^2 t. \quad (43)$$

One can see that the slopes of pyramids depend not only on the anisotropic surface free energy characterized by the coefficients  $m, a, b$  (as it would be in the case of a faceting transition of a thermodynamically unstable surface in the absence of kinetically controlled growth), but also on the driving force of the crystal growth, i.e., on the surface growth rate. This can be easily seen if one rewrites Eq. (42) for the asymptotic slope of the pyramid (antipyramid) edge in the dimensional variables,

$$(A^\pm)^2 = \frac{\bar{m} \mp \Delta_0 \sqrt{3\delta/(2\bar{a}\gamma_0^3)}}{\bar{b} + \bar{a}/3}, \quad (44)$$

where  $\bar{m}, \bar{a}, \bar{b}$  are the respective coefficients defined in Eq. (36) divided by  $\Gamma$ , i.e., the functions of the anisotropy coef-

ficients  $\epsilon_4$  and  $\epsilon_6$  only,  $\Delta_0$  is the surface-growth driving force, and  $\delta$  is the coefficient characterizing the additional energy of the pyramid edges and vertex defined in Eq. (12). If the thermodynamically unstable surface does not grow ( $\Delta_0=0$ ), the slopes of the facets that appear when the equilibrium is restored after the faceting transition are determined by the anisotropic surface free energy only, by means of the double-tangent construction. In our case a *dynamical slope*. This effect may be reminiscent of the phenomenon of a dynamic contact angle in a moving liquid-solid contact line [41,42]. It is important that the dynamical slopes of pyramids and antipyramids be *different*: the slope of a hill is *smaller* than the slope of a hole. This is due to the *convective* effect of the kinetically controlled surface growth discussed for a one-dimensional case in [17]: in the case of a concave surface (hole), the kinetically controlled growth tends to produce caustics and steepens the slope, while it tends to smooth the sharp corners and to reduce the slope in the case of a convex surface (hills). At the same time, the correction to the dimensionless unit growth speed of a planar surface in the laboratory frame,  $v^\pm = (A^\pm)^2$ , is smaller for pyramids and larger for antipyramids. Thus, faces of antipyramids propagate in the  $z$  direction faster than those of pyramids. This leads to the asymmetry between the pyramids and antipyramids that can be seen in Fig. 1. At the beginning of the structure formation both pyramids and antipyramids are present, but in the course of the surface growth antipyramids “grow out” and gradually disappear. A convective nature of the pyramid selection mechanism can be understood better if one considers infinitesimal perturbations of an almost planar pyramid face far from the vertex, where the surface is locally described as  $h = h_0 \sim A(x+y)$ . Indeed, taking  $h = h_0 + \tilde{h}$ , where the infinitesimal perturbation  $\tilde{h} \sim \exp[\sigma t + i(\alpha_x x + \alpha_y y)]$ , where  $\sigma$  is the perturbation growth rate and  $(\alpha_x, \alpha_y)$  is the perturbation wave vector, one obtains the following dispersion relation:

$$\sigma = \alpha^2 [m - A^2(a+b)] - c\alpha_x\alpha_y A^2 - \nu\alpha^4 + iA(\alpha_x + \alpha_y), \quad (45)$$

where  $\alpha^2 = \alpha_x^2 + \alpha_y^2$ . The last (imaginary) term on the right-hand side of the dispersion relation (45) shows that the disturbances of a pyramid (hill) travel from the vertex to the periphery, while the disturbances of an antipyramid move from the periphery to the vertex. Thus pyramids are sources of the perturbations and antipyramids are sinks. This accumulation of the perturbations descending from the pyramids into antipyramids eventually leads the disappearance of the latter.

Note that since the slopes of the pyramids do not change, their heights increase proportionally to their horizontal spatial scale in the course of the surface growth. The similar behavior caused by the existence of a “magic” slope remaining constant during the coarsening of square pyramidal mounds was observed experimentally in molecular-beam epitaxial growth [43] and reproduced in numerical simulations

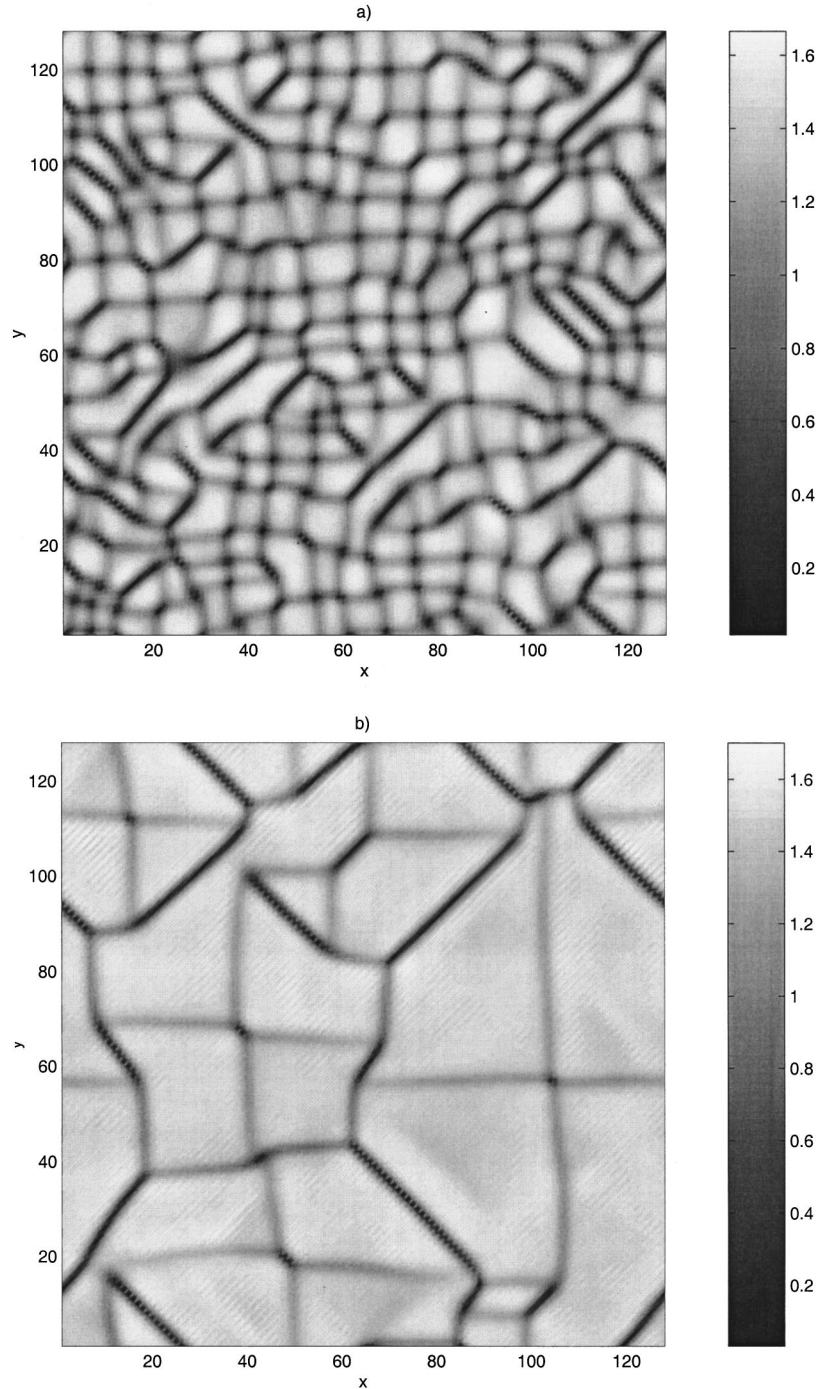


FIG. 2. Spatial distribution of the mean surface slope,  $|\nabla h|$ , corresponding to the numerical solution of Eq. (35) shown in Fig. 1, at two different times: a,  $t = 10^4$ ; b,  $t = 10^5$ . The spatial scale is arbitrary.

of the model proposed in [31] for the growth and coarsening of pyramidal structures caused by an anisotropic slope-dependent step current.

It should also be mentioned that if  $a \approx b$  in Eq. (35), the main nonlinear terms in Eq. (35) become almost rotationally invariant and the solution of Eq. (35) exhibits a labyrinthian hill-and-valley pattern similar to that produced by a two-dimensional isotropic Cahn-Hilliard equation [44]. Moreover, as one can see from Eqs. (42) and (44), solutions in the form of pyramids do not exist if  $m < \sqrt{3\nu/(2a)}$ , i.e., if

$$\Delta_0 > \bar{m} \sqrt{\frac{2a\gamma_0^3}{3\delta}}. \quad (46)$$

This corresponds to the case when the energy of the edges or the growth driving force is very large. Our preliminary numerical simulations of Eq. (35) in this case show an irregular pattern. We argue that the condition (46) may be related to the roughening transition.

### B. Orientation [111]

For the growth of the [111] surface, the anisotropy coefficients are

$$\begin{aligned}
 e_{20} &= e_{02} = \frac{1}{2} + \frac{3}{2} \epsilon_4 + \frac{25}{18} \epsilon_6, \\
 e_{40} &= e_{04} = -\frac{1}{72} (9 + 135 \epsilon_4 + 85 \epsilon_6), \\
 e_{22} &= -\frac{1}{4} \left( 1 + 15 \epsilon_4 + \frac{85}{9} \epsilon_6 \right), \\
 e_{21} &= -3 e_{03} = -2 \sqrt{2} \left( \epsilon_4 + \frac{5}{3} \epsilon_6 \right), \\
 e_{11} &= e_{12} = e_{30} = e_{31} = e_{13} = 0,
 \end{aligned} \tag{47}$$

and Eq. (20) reads

$$\begin{aligned}
 h_t &= \frac{1}{2} (\nabla h)^2 - m' \nabla^2 h - \nu \nabla^4 h + h_{xx} [d' h_y + a' h_x^2 + b' h_y^2] \\
 &\quad + h_{yy} [-d' h_y + b' h_x^2 + a' h_y^2] \\
 &\quad + 2 h_{xy} [d' h_x + (a' - b') h_x h_y],
 \end{aligned} \tag{48}$$

where

$$\begin{aligned}
 m' &= -\Gamma \left( 1 + 3 \epsilon_4 + \frac{25}{9} \epsilon_6 \right), \\
 a' &= -\Gamma \left( 1 + 21 \epsilon_4 + \frac{115}{9} \epsilon_6 \right), \\
 b' &= -\Gamma \left( 6 \epsilon_4 + \frac{10}{3} \epsilon_6 \right), \\
 d' &= -4 \sqrt{2} \Gamma (\epsilon_4 + 5 \epsilon_6 / 3).
 \end{aligned}$$

It can be easily checked that Eq. (48) is invariant with respect to rotations at the angles  $2\pi n/3$ . This corresponds to the threefold symmetry of a [111] surface of a cubic crystal. As above, consider the surface to be thermodynamically unstable, so one chooses  $\epsilon_4$  and  $\epsilon_6$  in such a way that  $m' > 0$ ;  $a$  and  $b$  are taken to be positive.

Figure 3 shows the numerical solution of Eq. (48) in a rectangular box with the  $y/x$  aspect ratio equal to  $\sqrt{3}/2$ . This aspect ratio was chosen in order to diminish the effect of the rectangular boundaries, breaking the threefold rotational symmetry, on the formation of the faceted structure. One can see the formation of the faceted structure consisting of triangular pyramids. Figures 3(a), 3(c), and 3(e) exhibit the shape of the crystal surface at different moments of time, and Figs. 3(b), 3(d), and 3(f) show the corresponding surface contour plots. At the initial stages the pyramids are slightly elongated in the  $y$  direction due to the effect of the boundaries, and their shape is distorted by mutual interaction. At the late stages the bases of the pyramids become equilateral. Such structure of triangular pyramids is observed in experiments on the faceting of unstable [111] surfaces caused by thermal

annealing [11–13], during the growth of Si(111) by gas phase epitaxy at high temperatures and by chemical vapor deposition [45,46], as well as during liquid phase epitaxial growth of  $\text{LiNbO}_3$  thick single-crystal films [47]. Evolution of the triangular pyramidal faceted structure on a growing [111] surface is the same as described above for the faceting of the growing [001] surface: after the structure with the horizontal length scale corresponding to the most unstable mode has been established, it coarsens with time; the pyramid slopes remain unchanged. Note that Eq. (48) is invariant with respect to transformation  $d \rightarrow -d$ ,  $y \rightarrow -y$ , and the pyramid orientation depends on the sign of the coefficient  $d$ . The structure with pyramids oriented opposite to those shown in Fig. 3 is shown in Fig. 4.

As in the case of square pyramids considered in the preceding subsection, the shape of the triangular pyramids with equilateral bases and their final slopes far from the vertices can be found analytically in a similar way. Indeed, consider a triangular pyramid with an equilateral basis oriented in such a way that the projection of one of its edges on the basis plane coincides with the negative part of the  $y$  axis (i.e., oriented as the pyramids shown in Fig. 4). The shape of the pyramid far from the vertex for  $y \rightarrow -\infty$  can be described by Eq. (37). A simple geometric consideration of the triangular pyramid with equilateral basis gives the following compatibility condition for the function  $f(x)$  in this case:

$$f'(\pm\infty) = \mp \sqrt{3}A. \tag{49}$$

Substitute Eq. (37) into Eq. (48), and obtain the following equation for  $f(x)$ :

$$\begin{aligned}
 \left( \frac{1}{2} A^2 - \nu \right) + \frac{1}{2} (f')^2 - (m - d'A - b'A^2) f'' \\
 + a' (f')^2 f''' - \nu f'''' = 0.
 \end{aligned} \tag{50}$$

Taking the same ansatz (40) for  $f'$ , one obtains from Eq. (50)

$$\begin{aligned}
 Q^2 &= \frac{3(m - d'A - b'A^2)}{a'} + \frac{3}{2a'} \sqrt{\frac{6\nu}{a'}} \operatorname{sgn} Q, \\
 k &= \sqrt{\frac{a'}{6\nu}} |Q|,
 \end{aligned} \tag{51}$$

where, as in the case considered in the preceding subsection, negative  $Q$  corresponds to a pyramid and positive  $Q$  corresponds to an antipyramid, respectively. From the compatibility condition,  $Q^2 = 3A^2$ , one obtains a quadratic equation for the slope of the triangular pyramid edge far from the vertex. A stable solution of this equation is determined by the sign of the coefficient  $d'$ . Namely,

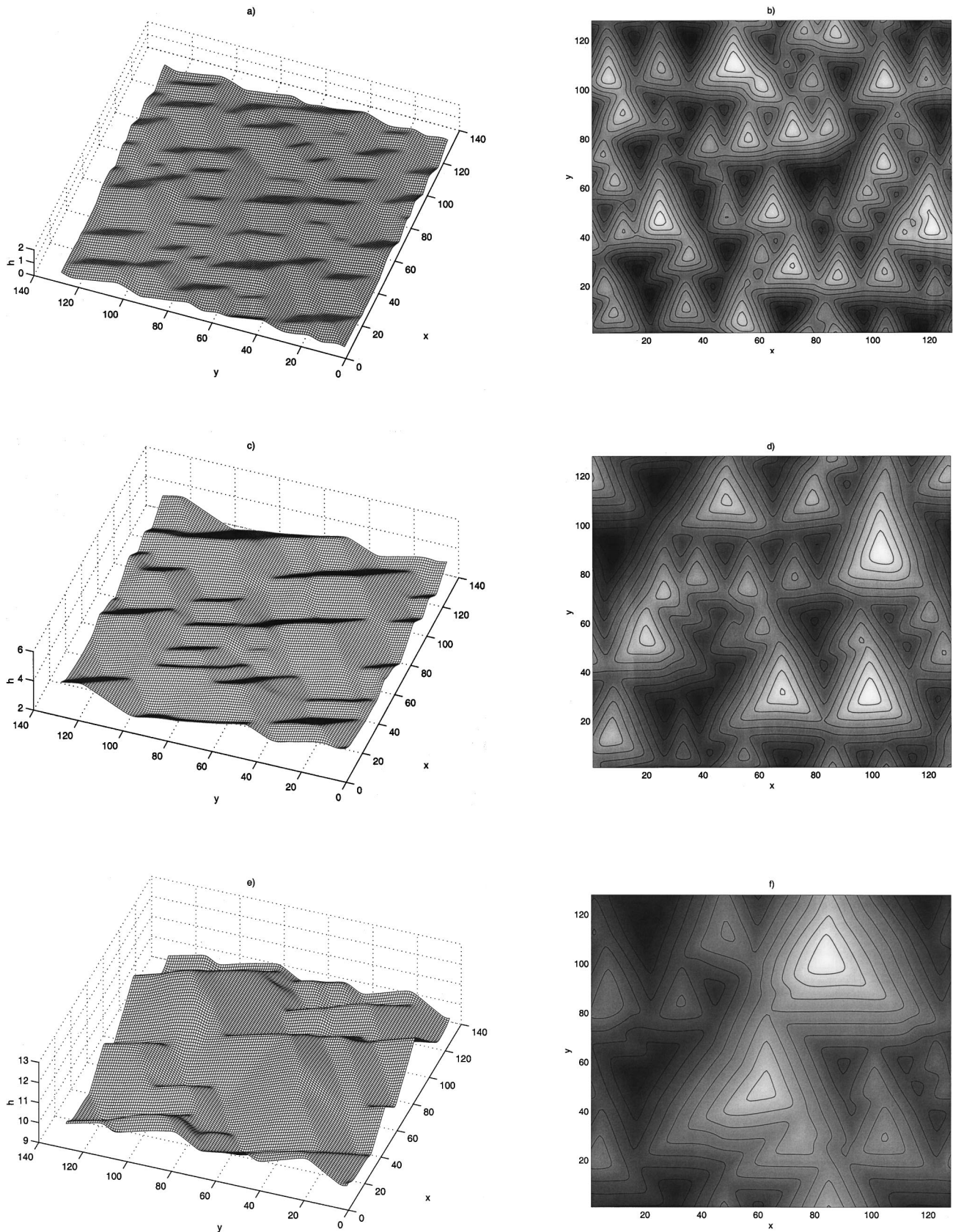


FIG. 3. Hill-and-valley structure on a growing crystal surface in the form of triangular pyramids: numerical solution of Eq. (48) at different moments of time: (a) and (b)  $t=10^4$ ; (c) and (d)  $t=4 \times 10^4$ ; (e) and (f)  $t=10^5$ ;  $m'=0.5$ ,  $\nu=0.001$ ,  $a'=1.0$ ,  $b'=0.1$ ,  $c'=1.8$ ,  $d'=0.5$ . The spatial scale is arbitrary.

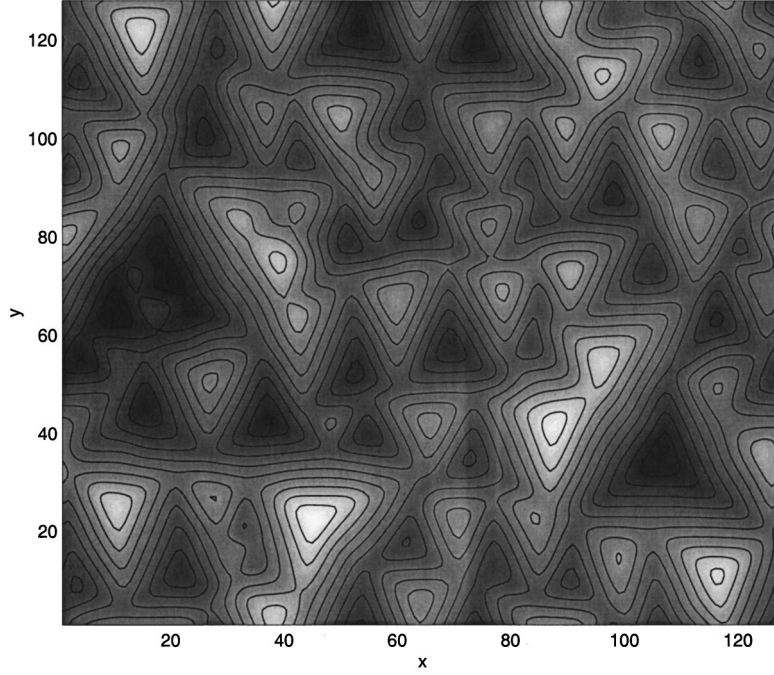


FIG. 4. Surface structure of triangular pyramids with the orientation opposite to that shown in Fig. 3, corresponding to a negative coefficient  $d'$  in Eq. (48) ( $m'=0.5$ ,  $\nu=0.001$ ,  $a'=1.0$ ,  $b'=0.1$ ,  $c'=1.8$ ,  $d'=-0.5$ ) for  $t=10^4$ . The spatial scale is arbitrary.

$$A^{\pm} = \frac{-d' - \sqrt{(d')^2 + 4(a'+b')[m' \mp \sqrt{3\nu/(2a')}]}}{2(a'+b')}$$

for  $d' > 0$ ,

(52)

$$A^{\pm} = \frac{-d' + \sqrt{(d')^2 + 4(a'+b')[m' \mp \sqrt{3\nu/(2a')}]}}{2(a'+b')}$$

for  $d' < 0$ ,

(53)

where  $A^{\pm}$  correspond to the hills ( $A^+$ ) and holes ( $A^-$ ), respectively. Thus, the shape of the triangular pyramids (antipyramids) for  $y \rightarrow -\infty$  is

$$h^{\pm}(x, y, t) \sim A^{\pm} y \mp \sqrt{\frac{6\nu}{a}} \ln \left[ \cosh \left( \sqrt{\frac{a}{2\nu}} |A^{\pm}| x \right) \right] + 2(A^{\pm})^2 t.$$
(54)

One can see that the parameters and evolution of triangular pyramids and antipyramids are distinguished, as discussed in the preceding subsection for the case of square pyramids. The solution in the form of triangular pyramids exists if  $(d')^2 + 4(a'+b')[m' - \sqrt{3\nu/(2a')}] > 0$ , i.e., as in the case of the square pyramids, the triangular pyramids can-

not form for large  $\nu$  corresponding to either very fast surface growth or to a large edge energy; these cases are not considered here.

### C. Orientation [110]

For this orientation one has

$$e_{20} = \frac{1}{2} + \frac{9}{4} \epsilon_4 + \frac{25}{8} \epsilon_6, \quad e_{02} = \frac{1}{2} - \frac{3}{4} \epsilon_4 - \frac{5}{8} \epsilon_6,$$

$$e_{22} \leq -\frac{1}{4} - \frac{21}{8} \epsilon_4 - \frac{115}{16} \epsilon_6,$$

$$e_{40} = -\frac{1}{8} - \frac{49}{16} \epsilon_4 - \frac{145}{32} \epsilon_6, \quad e_{04} = -\frac{1}{8} + \frac{31}{16} \epsilon_4 + \frac{35}{32} \epsilon_6,$$

$$e_{11} = e_{21} = e_{12} = e_{03} = e_{30} = e_{31} = e_{13} = 0.$$
(55)

Equation (20) in this case reads

$$h_t = \frac{1}{2} (\nabla h)^2 + h_{xx} [-m_x + a_x h_x^2 + b_x h_y^2] + h_{yy} [-m_y + a_y h_x^2 + b_y h_y^2] + \tilde{c} h_{xy} h_x h_y - \nu \nabla^4 h,$$
(56)

where

$$m_x = -\Gamma \left( \frac{9}{2} \epsilon_4 + \frac{25}{4} \epsilon_6 + 1 \right), \quad m_y = \Gamma \left( \frac{3}{2} \epsilon_4 + \frac{5}{4} \epsilon_6 - 1 \right),$$

$$a_x = -\Gamma \left( \frac{69}{2} \epsilon_4 + \frac{205}{4} \epsilon_6 + 1 \right),$$

$$b_x = -\Gamma \left( 3 \epsilon_4 + \frac{45}{4} \epsilon_6 \right),$$

$$a_y = -\Gamma (6 \epsilon_4 + 15 \epsilon_6), \quad b_y = \Gamma \left( \frac{45}{2} \epsilon_4 + \frac{25}{2} \epsilon_6 - 1 \right),$$

$$\tilde{c} = -\Gamma \left( 21 \epsilon_4 + \frac{115}{2} \epsilon_6 + 2 \right).$$

Here consider the anisotropy coefficients  $\epsilon_4$  and  $\epsilon_6$  to be such that the [110] surface is thermodynamically unstable in both  $x$  and  $y$  directions, i.e.,  $m_x > 0$  and  $m_y > 0$ . The other coefficients are also taken to be positive in our simulations.

Equation (56) is invariant with respect to transformations  $x \rightarrow -x$ ,  $y \rightarrow -y$ , but it is not invariant with respect to the transformation  $x \rightarrow y$ . This reflects the twofold symmetry of the [110] surface. Thus one can expect the faceting instability of this surface to result in the structure of either rhombic pyramids or grooves. One observes that the resulting structure depends on the degree of the anisotropy. Figure 5 shows the evolution of the faceted surface in the case when the asymmetry between the  $x$  and  $y$  directions is not very large, but the anisotropy is still large so that  $b_x/a_x$  and  $a_y/b_y$  are small. Figures 5(a), 5(c), 5(e), and 5(g) show the crystal surface shape at different moments of time, and Figs. 5(b), 5(d), 5(f), and 5(h) exhibit the corresponding surface contour plots. First one observes the formation of a system of grooves [Figs. 5(a) and 5(b)]. Later, the grooves decay into islands in the form of rhombic pyramids [Figs. 5(c) and 5(d)]. Similar rhombic pyramids are observed, e.g., during the epitaxial growth of an In-Ga-As alloy on the InP(001) surface [48]. The rhombic pyramids coarsen in time [Figs. 5(e)–5(h)], but while the shapes of the square and triangular pyramids remain self-similar during the coarsening, the coarsening rates of the rhombic pyramids are different in the  $x$  and  $y$  directions. Namely, one observes that the coarsening in the  $y$  direction goes a little faster, so that the rhombic pyramids gradually thicken in the  $y$  direction (see Sec. VI) and tend to a limiting rhombic shape that can be found analytically for regions far from the vertex in a way similar to that described in the preceding subsections for the square and triangular pyramids. Indeed, consider a rhombic pyramid oriented in such a way that the projections of its edges on the basis plane coincide with the  $x$  and  $y$  axes. For the asymptotics of the pyramid shape far from the vertex one has

$$\begin{aligned} h &\sim Ax + f(y) + vt, \quad f'(\pm\infty) = \mp B \quad \text{as } x \rightarrow -\infty, \\ h &\sim By + g(x) + vt, \quad g'(\pm\infty) = \mp A \quad \text{as } y \rightarrow -\infty. \end{aligned} \quad (57)$$

Taking  $f'(y) = Q_y \tanh k_y y$ ,  $g'(x) = Q_x \tanh k_x x$ , one obtains from Eq. (56)

$$\begin{aligned} k_y &= \sqrt{\frac{b_y}{6\nu}} |Q_y|, \quad Q_y^2 = \frac{3(m_y - a_y A^2)}{b_y} + \frac{3}{2b_y} \sqrt{\frac{6\nu}{b_y}} \operatorname{sgn} Q_y, \\ k_x &= \sqrt{\frac{a_x}{6\nu}} |Q_x|, \quad Q_x^2 = \frac{3(m_x - b_x B^2)}{a_x} + \frac{3}{2a_x} \sqrt{\frac{6\nu}{a_x}} \operatorname{sgn} Q_x, \end{aligned} \quad (58)$$

where, as before, negative (positive)  $Q_{x,y}$  correspond to pyramids (antipyramids). The compatibility conditions  $Q_x^2 = A^2$ ,  $Q_y^2 = B^2$  yield a system of linear equations for squares of the limiting slopes of the pyramid edges in the  $x$  and  $y$  directions,  $A^2$  and  $B^2$ , respectively, whose solution gives

$$(A^\pm)^2 = \frac{9b_x[m_y \mp \sqrt{3\nu/(2b_y)}] - 3b_y[m_x \mp \sqrt{3\nu/(2a_x)}]}{9a_y b_x - a_x b_y}, \quad (59)$$

$$(B^\pm)^2 = \frac{9a_y[m_x \mp \sqrt{3\nu/(2a_x)}] - 3a_x[m_y \mp \sqrt{3\nu/(2b_y)}]}{9a_y b_x - a_x b_y}.$$

The superscripts  $+$  and  $-$  correspond to pyramids and anti-pyramids, respectively. Thus the functions  $f(y)$  and  $g(x)$  describing the asymptotic shape of the rhombic pyramids in Eqs. (57) are

$$f^\pm(y) = \mp \sqrt{\frac{6\nu}{b_y}} \ln \left[ \cosh \left( \sqrt{\frac{b_y}{6\nu}} |B^\pm| x \right) \right], \quad (60)$$

$$g^\pm(x) = \mp \sqrt{\frac{6\nu}{a_x}} \ln \left[ \cosh \left( \sqrt{\frac{a_x}{6\nu}} |A^\pm| x \right) \right],$$

and the nonlinear correction for the growth speed  $v^\pm = \frac{1}{2}[(A^\pm)^2 + (B^\pm)^2]$ . Obviously, the solution for the square pyramids described above is the particular case of the rhombic pyramids for  $m_x = m_y = m$ ,  $a_x = b_y = a$ ,  $a_y = b_x = b$ ,  $A = B$ .

Note that Eqs. (59) have real solutions provided the right-hand sides of the two equations are positive. Thus, for  $\nu \ll 1$ , the rhombic pyramids can be formed if

$$\frac{9b_x m_y - 3b_y m_x}{9a_y b_x - a_x b_y} > 0, \quad \frac{9a_y m_x - 3a_x m_y}{9a_y b_x - a_x b_y} > 0. \quad (61)$$

Otherwise, one obtains the solution in the form of grooves rather than rhombic pyramids. Numerical solution of Eq. (56) in this case is shown in Fig. 6 [Figs. 6(a), 6(c), 6(e), and 6(g) show the crystal surface shape at different times, and Figs. 6(b), 6(d), 6(f), and 6(h) show the corresponding surface contour plots]. The grooves do not decay into pyramidal islands, and in a finite periodic box the structure ultimately becomes quasi-one-dimensional. The groove slope does not

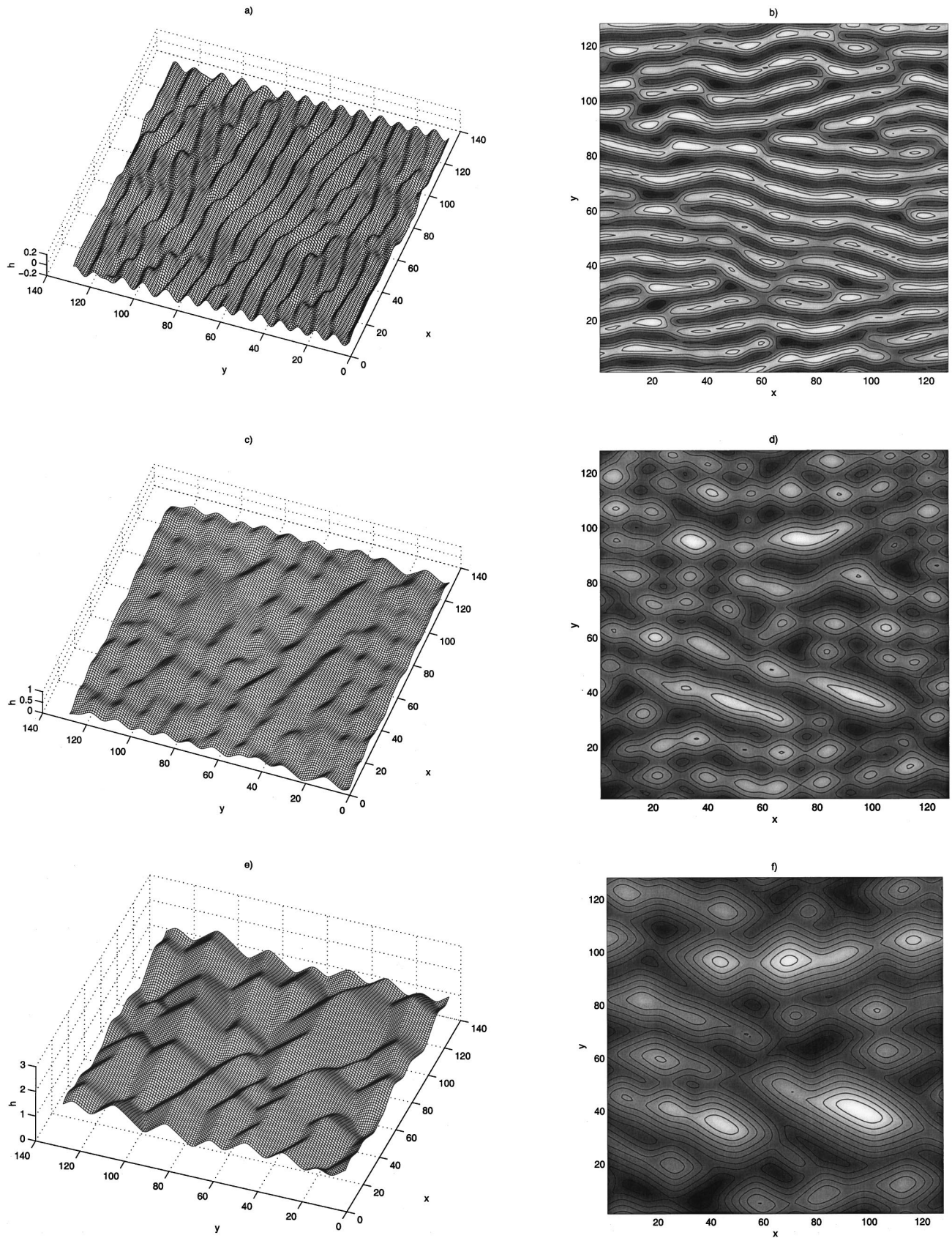


FIG. 5. Hill-and-valley structure on a growing crystal surface in the form of rhombic pyramids: numerical solution of Eq. (56) at different moments of time: (a) and (b)  $t=2 \times 10^3$ ; (c) and (d)  $t=10^4$ ; (e) and (f)  $t=3 \times 10^4$ ; (g) and (h)  $10^5$ ;  $m_x=0.3$ ,  $m_y=0.5$ ,  $a_x=1.0$ ,  $b_x=0.1$ ,  $a_y=0.2$ ,  $b_y=0.8$ ,  $\tilde{c}=0.3$ ,  $\nu=0.001$ . The spatial scale is arbitrary.

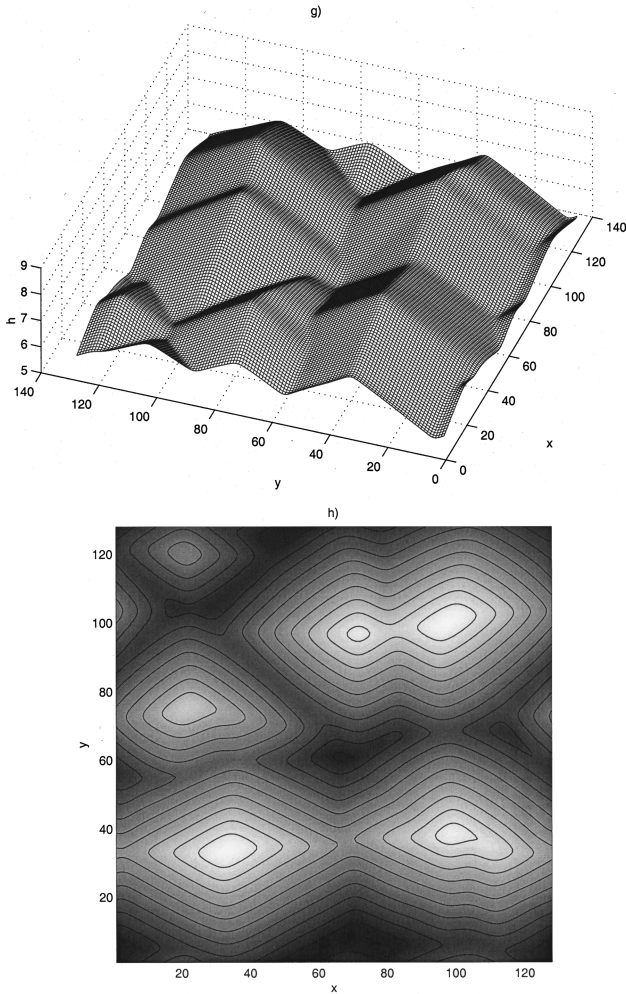


FIG. 5 (Continued).

change during the coarsening. Formation and coarsening of the system of grooves similar to those shown in Fig. 6 are observed, e.g., during the faceting of thermodynamically unstable (0001) and  $\{10\bar{1}0\}$  surfaces of  $\text{Al}_2\text{O}_3$  caused by thermal annealing [49], as well as in the course of unstable homoepitaxial growth of  $\text{GaAs}(001)$  [50]. The coarsening rates in the  $x$  and  $y$  directions differ more than in the case of rhombic pyramids. The anisotropy of the coarsening rates is studied in Sec. VI.

#### D. Exact solutions

In the preceding subsections we have numerically studied the formation of square and rhombic pyramids in the cases when either  $b/a$  or  $b_x/a_x$  and  $a_y/b_y$  were numerically small (large anisotropy). It turns out that if  $b=0$  in Eq. (35), or if  $b_x=a_y=0$  in Eq. (56), it is possible to construct the *exact* solutions of Eqs. (35) and (56). First consider the latter case which is more general. In this case one can seek for the solution of Eq. (56) in the form

$$h(x,y,t) = f(x) + g(y) + vt. \quad (62)$$

Substituting Eq. (62) in Eq. (56) one obtains two decoupled equations for  $f$  and  $g$  whose solutions are described above.

Thus, one obtains the following exact solution of Eq. (56) for  $b_x=a_y=0$  in the form of a rhombic pyramid or antipyrmaid:

$$h^\pm(x,y,t) = \mp \sqrt{\frac{6\nu}{a_x}} \ln(\cosh k_x^\pm x) \mp \sqrt{\frac{6\nu}{b_y}} \ln(\cosh k_y^\pm y) + v^\pm t, \quad (63)$$

$$k_x^\pm = \sqrt{\frac{m_x}{2\nu} \mp \sqrt{\frac{3}{8\nu a_x}}}, \quad k_y^\pm = \sqrt{\frac{m_y}{2\nu} \mp \sqrt{\frac{3}{8\nu b_y}}},$$

$$v^\pm = \frac{3}{2} \left( \frac{m_x}{a_x} + \frac{m_y}{b_y} \right) \mp \frac{3\sqrt{6\nu}}{4} (a_x^{-3/2} + b_y^{-3/2}),$$

where the superscript  $+$  corresponds to pyramids and  $-$  to antipyramids. The exact solution (63) in the form of a rhombic pyramid is shown in Fig. 7(a).

The exact solution in the form of square pyramids is obtained from Eq. (63) by setting  $m_x=m_y=m$ ,  $a_x=b_y=a$ . One gets

$$h^\pm(x,y,t) = \mp \sqrt{\frac{6\nu}{a}} \ln(\cosh k^\pm x \cosh k^\pm y) + v^\pm t, \quad (64)$$

$$k^\pm = \sqrt{\frac{m}{2\nu} \mp \sqrt{\frac{3}{8\nu a}}}, \quad v^\pm = \frac{3}{a} \left( m \mp \sqrt{\frac{3\nu}{2a}} \right).$$

The exact solution (64) in the form of a square pyramid is shown in Fig. 7(b).

## VI. COARSENING RATE

In many systems the coarsening of the structures resulting from instabilities is known to go with time  $t$  at late stages obeying a power law, i.e.,  $L(t) \sim t^\alpha$ , where  $L$  is the characteristic length scale of the structure [51,21] and  $\alpha$  is the coarsening exponent. These have been measured for the growth of thermodynamically unstable [001], [111], and [110] surfaces. Square and triangular pyramids corresponding to the faceting of growing [001] and [111] surfaces, respectively, remain self-similar during the coarsening, so that the coarsening rates in the  $x$  and  $y$  directions were the same. For this case the characteristic scale of the structure was computed in two ways:  $L_1(t) = N^{-1} \sum_{i=1}^N Z_i^{-1}(t)$ , where  $N$  is the number of collocation points ( $N=128$  in our case) and  $Z_i(t)$  is the number of zeros of the function  $h(x,y_i,t)$  on the  $i$ th  $y$  layer, and  $L_2(t) = N_+(t)/N_0(t)$ , where  $N_+$  is the number of spatial points where  $h(x,y,t) - \bar{h}(t) > 0$  and  $N_0$  is the number of points where  $h - \bar{h} = 0$  ( $\bar{h}$  is the spatially mean value of  $h$  which is equal to the zeroth Fourier mode). It was found that  $L_1(t)$  and  $L_2(t)$  are proportional to each other and thus both measures of the characteristic spatial scale of the structure are equivalent.

Figure 8 shows the growth of the characteristic spatial scale of square and triangular pyramids (squares and triangles, respectively). The results with random initial data are averaged over ten realizations. One can see the formation of the initial periodic structure after the characteristic time of linear instability, and the transition to the power-law coarsening.

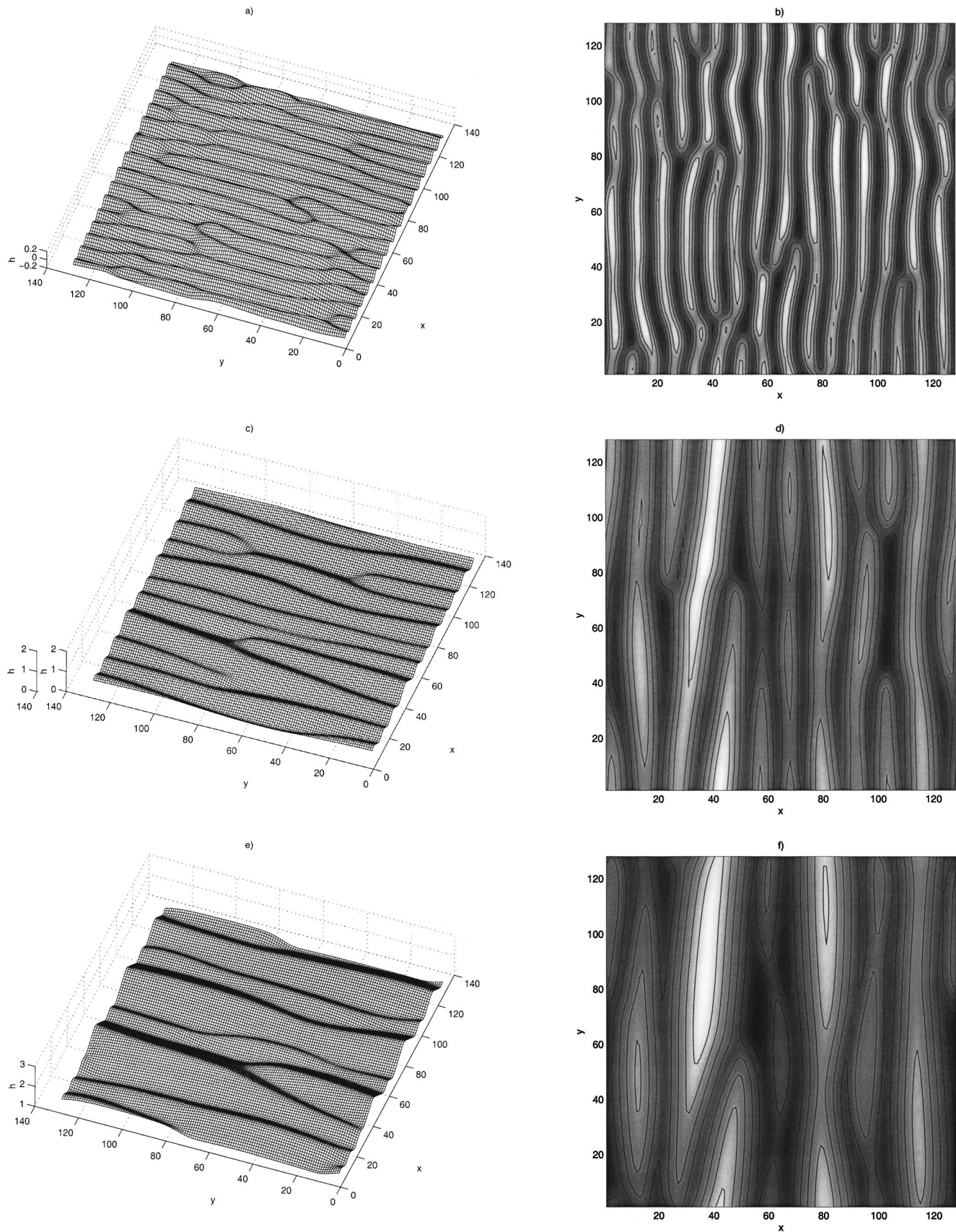


FIG. 6. Hill-and-valley structure on a growing crystal surface in the form of grooves: numerical solution of Eq. (56) at different moments of time: (a) and (b)  $t=2 \times 10^3$ ; (c) and (d)  $t=2 \times 10^4$ ; (e) and (f)  $t=4 \times 10^4$ ; (g) and (h)  $t=10^5$ ;  $m_x=0.5$ ,  $m_y=0.1$ ,  $a_x=1.0$ ,  $b_x=0.1$ ,  $a_y=0.2$ ,  $b_y=0.8$ ,  $\tilde{c}=0.3$ ,  $\nu=0.001$ . The spatial scale is arbitrary.

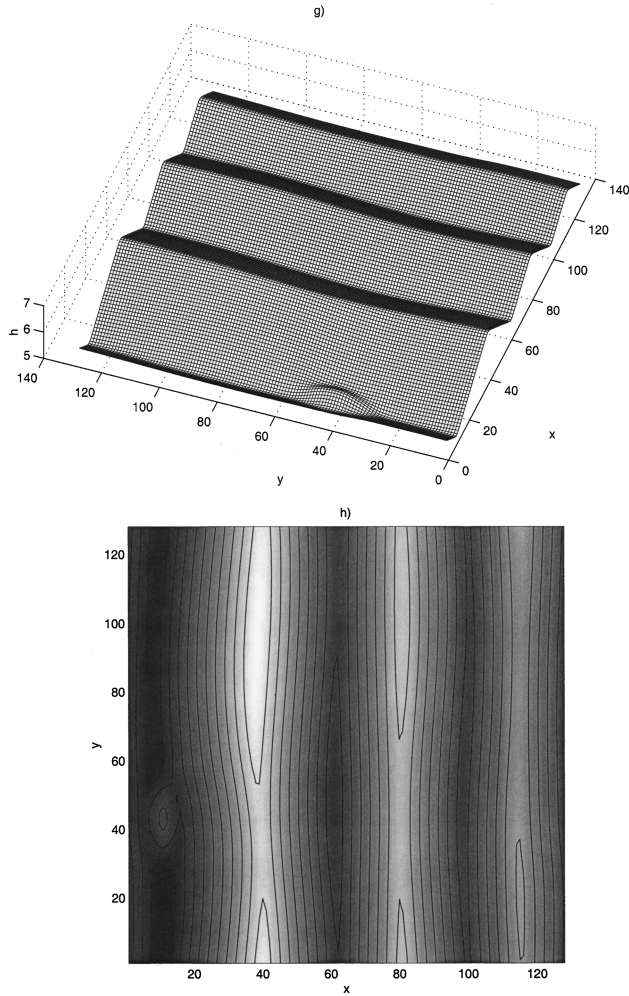


FIG. 6 (Continued).

ening at the late stage shown in detail in the inset. The coarsening exponent  $\alpha$  was measured to be 0.47 for square pyramids and 0.45 for triangular pyramids, i.e., practically the same. Similar exponents, 0.4 and  $0.42 \pm 0.4$ , were observed in experiments on coarsening of square pyramids in homolayer and multilayer epitaxial growth of Ge(001) [39,40]. The exponents obtained in the computations are considerably larger than those corresponding to the coarsening of faceted thermodynamically unstable surfaces when there is *no* kinetically controlled surface growth. In this case the coarsening rate depends on the mechanism of the surface reconstruction, and theoretical predictions give  $1/4$  for the evaporation-condensation mechanism and  $1/6$  for the surface-diffusion mechanism [21], which is confirmed by numerical computations [9]. Slow coarsening with the exponents  $1/4$  and  $1/6$  was also obtained, theoretically and experimentally, in different problems of epitaxial growth and molecular-beam epitaxy (see [21] for review). The present exponents are closer to that predicted by Mullins for the evaporation-condensation mechanism, i.e.,  $1/2$  [15]. One can attribute the fast coarsening in our case to the convective effect of kinetics which governs the growth of the crystal surface. Convective effects are known to increase the rate of coarsening in various problems of spinodal decomposition in phase separating systems (see [51] for review).

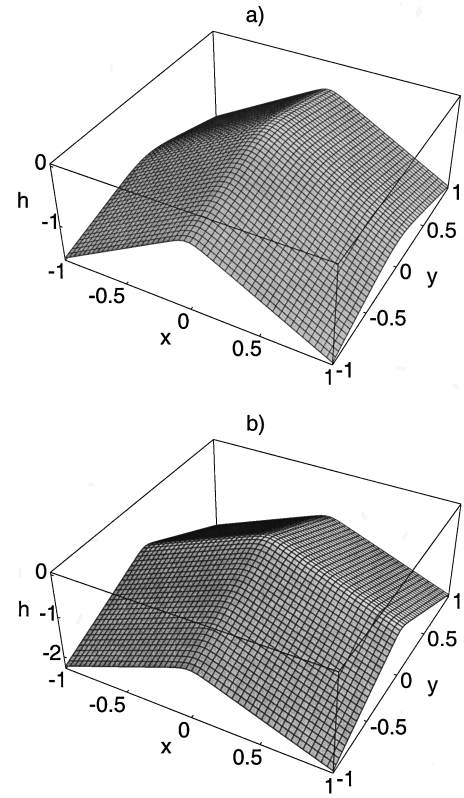


FIG. 7. (a) Exact solution (63) of Eq. (56) for  $m_x=0.5$ ,  $m_y=0.1$ ,  $a_x=1.0$ ,  $b_y=0.4$ ,  $\nu=0.001$ ,  $a_y=b_x=0$ , in the form of a rhombic pyramid. (b) Exact solution (64) of Eq. (35) for  $m=0.5$ ,  $a=1.0$ ,  $\nu=0.001$ ,  $b=0$ , in the form of a square pyramid.

As has been already mentioned, it was found that the rate of coarsening of the faceted structure resulting from the faceting instability of the growing [110] surface is anisotropic, i.e., the growth rates of the structure spatial scales are different in  $x$  and  $y$  directions. For this case the length scales  $\langle L_x \rangle$  and  $\langle L_y \rangle$  in the  $x$  and  $y$  directions, respectively, are separately measured as  $\langle L_{x,y} \rangle = N^{-1} \sum_{i=1}^N 2(n_x, n_y)_i^+ / Z_i$ , where  $(n_x)_i^+ [(n_y)_i^+]$  are the number of points in the  $i$ th  $x$  ( $y$ ) layer where  $h - \bar{h}$  is positive, and  $Z_i$  is the number of zeros of  $h - \bar{h}$  in the  $i$ th  $x$  or  $y$  layer. Figure 9 shows the coarsening of anisotropic faceted structures for the two cases studied in the preceding section, namely, for rhombic pyramids (diamonds) and for grooves (circles). The two curves for each structure correspond to the  $x$  and  $y$  directions in the surface plane; the results are averaged over ten realizations with different random initial data. The power-law coarsening regime is shown in detail in the inset. The coarsening exponents were found to be 0.61 and 0.41 for rhombic pyramids and 0.57 and 0.23 for grooves. Note that anisotropic facets coarsening was studied theoretically [52] and experimentally [53] for the case of the faceting transition of the thermally quenched crystal surface when the rate-limiting mechanism of facet growth was collisions between step bunches. The coarsening exponents were computed to be  $1/6$  and  $1/2$  for the grooves' characteristic width and length, respectively. This was confirmed in recent experiments with the faceting of the Si(113) surface, for which the exponents for the groove coarsening were found to be 0.164 for the groove width and 0.44 for the groove length [53]. In our case the

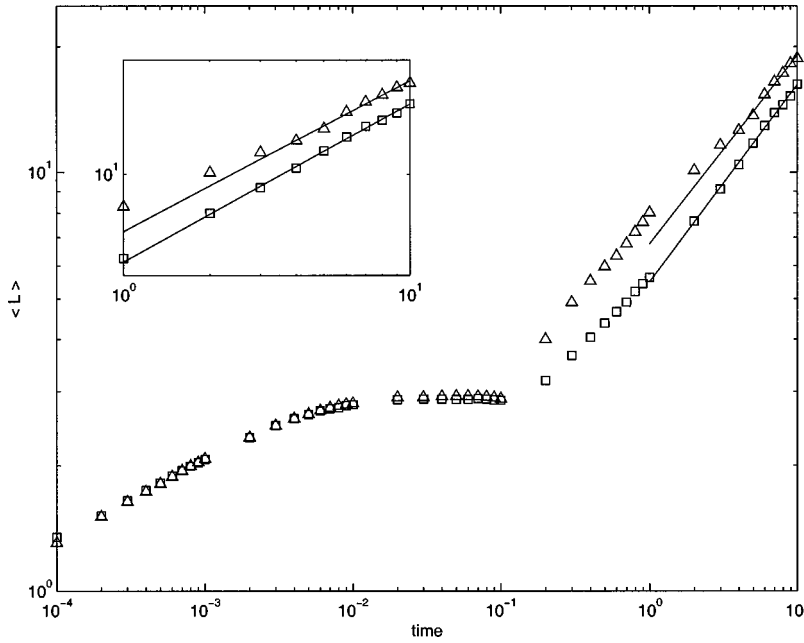


FIG. 8. The increase of the mean horizontal spatial scale (in arbitrary units) of the faceted surface structures in the form of square (squares) and triangular (triangles) pyramids corresponding to the numerical solutions of Eqs. (35) and (48), respectively. The inset shows the power-law regime at the late stage of the coarsening.

groove length also grows much faster in the beginning of the groove formation, but in the power-law regime it grows slower than the groove widths, approaching the limit determined by the computational domain. In the power-law regime the coarsening exponents are found to be  $\alpha=0.23$  for groove length and  $\alpha=0.57$  for groove width. After the groove length has reached the computational domain limit, the structure becomes effectively one-dimensional and its coarsening is governed by the exponent characterizing the growth of the groove width. This exponent, in the considered

highly anisotropic case, is close to the value of 1/2 found for the one-dimensional case [17].

### VII. EFFECT OF THERMAL DIFFUSION BOUNDARY LAYER

In order to study the effect of the thermal diffusion boundary layer on the faceting instability of a growing thermodynamically unstable crystal surface, one can solve Eq. (32) numerically for the case of the [001] surface. In this

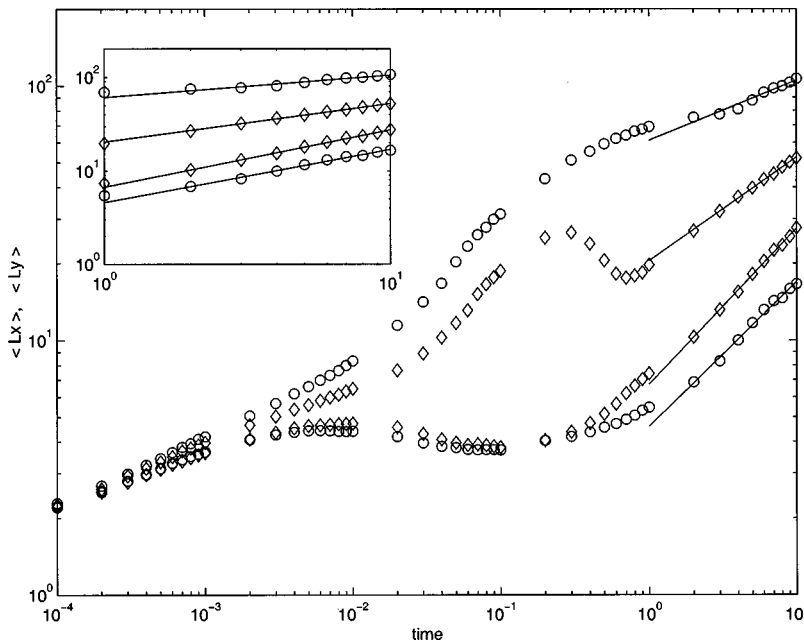


FIG. 9. The increase of the mean horizontal spatial scales (in arbitrary units) in  $x$  and  $y$  directions of the faceted surface structures in the form of rhombic pyramids (rhombs) and grooves (circles) corresponding to the numerical solutions of Eq. (56). The inset shows the power-law regime at the late stage of the coarsening.

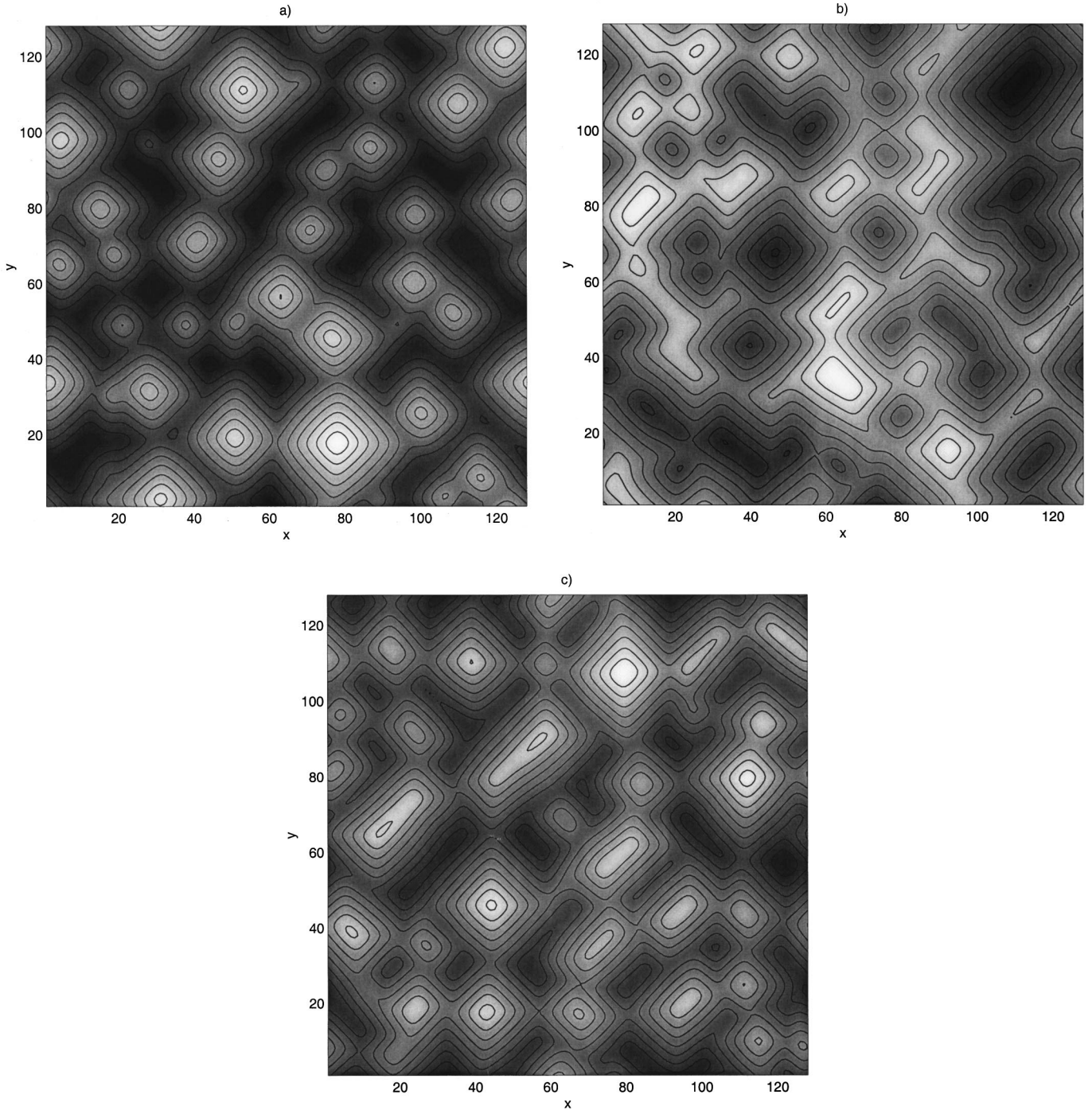


FIG. 10. Solutions of Eq. (32) corresponding to the growth of the unstable [001] surface for  $\mu_{11}^s = \mu_{22}^s = 0.5$ ,  $a_{11}^s = b_{22}^s = 1.0$ ,  $b_{11} = a_{22} = 0.1$ ,  $c_{12}^s = 0.3$ ,  $\chi_{1111} = \chi_{2222} = 3\chi_{1122} = 0.05$ , and different values of  $g$ : (a)  $g = 0.05$ , (b)  $g = -0.05$ , (c)  $g = 0.0$ . Other coefficients in Eq. (32) are equal to zero. The spatial scale is arbitrary.

case Eq. (32) differs from Eq. (35) only by the term with the Gaussian curvature,  $g \partial(h_x, h_y) / \partial(x, y)$ , on the right-hand side. It can be seen for the solidification of a hypercooled melt in a thermodynamically unstable direction that the coefficient  $g$  is negative. However, since for some other systems  $g$  might also be positive, both cases have been studied.

Figure 10 shows the structure forming from the unstable growing planar surface for  $g > 0$  [Fig. 10(a)],  $g < 0$  [Fig. 10(b)], and  $g = 0$  [Fig. 10(c)]. One can see that for  $g > 0$  the pyramids are more rounded looking more like “square” cones. Such rounded square pyramids as well as almost

rounded cones are observed in some epitaxial growth systems [54]. It is thus conceivable that the rounding of the pyramid edges in the course of epitaxial growth can be caused by the effect of interaction between the thermal or concentration field and the shape of the crystal surface (if the growth is controlled by the evaporation-condensation mechanism).

For  $g < 0$  [Fig. 10(b)], instead of cones one can see now square rounded holes forming on a growing thermodynamically unstable surface. Square, triangular, and spiral holes on the crystal surface are observed in experiments when the

crystal surface is evaporating [55–57], and they are believed to be caused by the dislocations meeting the crystal surface. We are not aware of any experimental observations of the formation of holes on a growing crystal surface. However, since the considered model of surface growth is proposed for the evaporation-condensation mechanism, such effects of mass or heat transfer in diffusion boundary layers near the crystal surfaces are conceivable.

It should be noted, however, that the numerical solutions of Eq. (32) always blow up after a certain time interval. It is difficult to determine whether it was purely numerical instability or an intrinsic property of the equation. The latter is possible since the nonlinear evolution equation describing the *morphological* instability of the uniformly propagating solidification front in a hypercooled melt derived in [36] and containing the term with the Gaussian curvature was proved to exhibit the self-similar blow-up [58]. This question is left for further investigation.

### VIII. DISCUSSION AND CONCLUSIONS

A phenomenological equation has been proposed for the modeling of the formation of facets and corners during the growth of a thermodynamically unstable crystal surface in the case when the crystal growth is controlled by the attachment kinetics, evaporation-condensation is the dominant transport mechanism, and the faceting is caused by strongly anisotropic surface tension. The general form of the equation for the surface shape  $h$  contains, in particular cases, the equations which describe the faceting of growing [001], [111], and [110] surfaces. The equation was solved numerically for these particular cases and the solutions for  $h$  in the form of square pyramids ([001]), triangular pyramids ([111]), as well as rhombic pyramids and grooves ([110]) were found. The nonlinear evolution of the faceted structures is similar in all the cases, namely, after formation the pyramids or grooves have a characteristic slope which remains unchanged while the structure coarsens in time and at the late stages obey a power law  $L(t) \sim t^\alpha$ , where  $L(t)$  is the characteristic horizontal spatial scale and  $\alpha$  is the coarsening exponent. It was found that  $\alpha$  is practically the same for square and triangular pyramids. In addition, the coarsening of the [110] faceted surface was observed to be anisotropic, so that the characteristic lengths in the  $x$  and  $y$  directions have different coarsening exponents.

The final slope of the pyramids far from the vertex was found analytically. It was shown that, due to the effect of the attachment kinetics, the *dynamic* slope of the pyramid is determined by both the anisotropic surface tension and the growth driving force. The convective nature of this effect makes the slope of the pyramids (hills) smaller than the slope of the antipyramids (holes), and leads to the elimination of

antipyramids in the course of the surface growth. For some particular cases the *exact* solutions are found describing the shape of the growing surface in the form of square and rhombic pyramids. The selection conditions for rhombic pyramids and grooves were found analytically.

A more general case was considered where there is a feedback between the evolution of the crystal surface shape and the thermal or concentration field near the surface. Taking solidification in a hypercooled melt as an example, an evolution equation is derived for the growing crystal surface in the diffusion boundary-layer approximation. The resulting equation is similar to that mentioned above, but contains an additional term proportional to the Gaussian curvature of the surface. The numerical simulations show that, depending on the sign of the coefficients of this term, it yields the formation of either rounded pyramids or rounded holes on the growing surface.

The variety of solutions of the derived equations resembles many structures observed in experiments on faceting of thermodynamically unstable surfaces, as well as on vapor and liquid phase epitaxial growth and chemical vapor deposition. One should note that the experimental conditions under which the pyramidal structures were observed did not always correspond to the evaporation-condensation mechanism of the surface growth. In many cases the governing mechanism of the pyramid growth is connected with surface diffusion, slope-dependent flow of steps, elastic stresses caused by the misfit of the crystal lattices of the substrate and the growing solid film, etc. These mechanisms, strictly speaking, require a special consideration, and the evolution equation for the surface shape can be altered when different mechanisms are present. However, the derived equation has several important properties which may be applicable to a larger class of systems. First, it correctly reflects the symmetries of the growing crystal surface and leads to the formation of structures seen in many experiments. Second, the nonlinear behavior of the solutions, namely, the saturation of the pyramid and groove slopes, the power-law coarsening at the late stages, as well as anisotropic coarsening for surfaces with certain symmetries, is also observed in many experiments with different surface-growth mechanisms [32].

### ACKNOWLEDGMENTS

This work was supported by a grant from the National Aeronautics and Space Administration, Program on Microgravity Sciences and Applications. We are grateful to Professor P.W. Voorhees for numerous fruitful discussions. We are indebted to Professor M. Matalon, Professor H. Riecke, and Professor V. Volpert for sharing their computational resources with us.

### APPENDIX

Here we reproduce the coefficients  $e_{ij}(\theta, \phi, \epsilon_4, \epsilon_6)$ , defined in Eq. (13), characterizing the anisotropy of the free energy of a crystal surface with the orientation  $\{\sin \theta \cos \phi, \sin \theta \sin \phi, \cos \theta\}$ , computed in [25]:

$$e_{00} = 1 + \epsilon_4 \left( \cos(\theta)^4 + \frac{1}{4} [3 + \cos(4\phi)] \sin(\theta)^4 \right) + \epsilon_6 \left( \cos(\theta)^6 + \frac{1}{8} [5 + 3 \cos(4\phi)] \sin(\theta)^6 \right),$$

$$\begin{aligned}
e_{10} &= \frac{1}{4} \{-4 \epsilon_4 - 3 \epsilon_6 [1 - \cos(2 \theta)]\} \sin(4 \phi) \sin(\theta)^3, \\
e_{01} &= \left[ 2 \epsilon_4 \left( \cos(\theta)^2 - \frac{1}{4} [3 + \cos(4 \phi)] \sin(\theta)^2 \right) + 3 \epsilon_6 \left( \cos(\theta)^4 - \frac{1}{8} [5 + 3 \cos(4 \phi)] \sin(\theta)^4 \right) \right] \sin(2 \theta), \\
e_{20} &= \frac{1}{2} - \frac{3}{2} \epsilon_4 \left( \cos(\theta)^4 - 2 \sin(2 \phi)^2 \sin(\theta)^2 + \frac{1}{4} [3 + \cos(4 \phi)] \sin(\theta)^4 \right) \\
&\quad - \frac{5}{2} \epsilon_6 \left( \cos(\theta)^6 - \frac{3}{2} \sin(2 \phi)^2 \sin(\theta)^4 + \frac{1}{8} [5 + 3 \cos(4 \phi)] \sin(\theta)^6 \right), \\
e_{11} &= \frac{3}{4} \cos(\theta) \{4 \epsilon_4 + 5 \epsilon_6 [1 - \cos(2 \theta)]\} \sin(4 \phi) \sin(\theta)^2, \\
e_{02} &= \frac{1}{2} - \frac{3}{2} \epsilon_4 \left[ \cos(\theta)^4 + \frac{1}{4} [3 + \cos(4 \phi)] \sin(\theta)^4 - \left( 1 + \frac{1}{4} [3 + \cos(4 \phi)] \right) \sin(2 \theta)^2 \right] \\
&\quad - \frac{5}{2} \epsilon_6 \left[ \cos(\theta)^6 + \frac{1}{8} [5 + 3 \cos(4 \phi)] \sin(\theta)^6 - \frac{3}{2} \left( \cos(\theta)^2 + \frac{1}{8} [5 + 3 \cos(4 \phi)] \sin(\theta)^2 \right) \sin(2 \theta)^2 \right], \\
e_{30} &= \frac{1}{4} \{ \epsilon_4 [7 - 3 \cos(2 \theta)] + 15 \epsilon_6 \sin(\theta)^4 \} \sin(4 \phi) \sin(\theta), \\
e_{21} &= 3 \epsilon_4 \left( -\cos(\theta)^2 - \sin(2 \phi)^2 + \frac{1}{4} [3 + \cos(4 \phi)] \sin(\theta)^2 \right) \sin(2 \theta) \\
&\quad + \frac{15}{2} \epsilon_6 \left( -\cos(\theta)^4 - \sin(2 \phi)^2 \sin(\theta)^2 + \frac{1}{8} [5 + 3 \cos(4 \phi)] \sin(\theta)^4 \right) \sin(2 \theta), \\
e_{12} &= -\frac{3}{32} \{8 \epsilon_4 [1 + 3 \cos(2 \theta)] + 5 \epsilon_6 [1 + 4 \cos(2 \theta) - 5 \cos(4 \theta)]\} \sin(4 \phi) \sin(\theta), \\
e_{03} &= \epsilon_4 \left( -3 \cos(\theta)^2 + 2 \sin(\theta)^2 + \frac{1}{4} [3 + \cos(4 \phi)] [-2 \cos(\theta)^2 + 3 \sin(\theta)^2] \right) \sin(2 \theta) \\
&\quad + \frac{5}{2} \epsilon_6 \sin(2 \theta) \left( -3 \cos(\theta)^4 + \sin(2 \theta)^2 + \frac{1}{8} [5 + 3 \cos(4 \phi)] [3 \sin(\theta)^4 - \sin(2 \theta)^2] \right), \\
e_{40} &= -\frac{1}{8} + \epsilon_4 \left[ \frac{15}{8} \cos(\theta)^4 - \frac{9}{2} \sin(2 \phi)^2 \sin(\theta)^2 + \frac{1}{4} [3 + \cos(4 \phi)] \left( 1 + \frac{15}{8} \sin(\theta)^4 \right) \right] \\
&\quad + \epsilon_6 \left[ \frac{35}{8} \cos(\theta)^6 + \frac{35}{64} [5 + 3 \cos(4 \phi)] \sin(\theta)^6 + \frac{15}{4} \sin(2 \phi)^2 \sin(\theta)^2 \left( 1 - \frac{5}{2} \sin(\theta)^2 \right) \right], \\
e_{31} &= -\frac{1}{4} \cos(\theta) \{ \epsilon_4 [13 - 9 \cos(2 \theta)] + 75 \epsilon_6 \sin(\theta)^4 \} \sin(4 \phi), \\
e_{22} &= -\frac{1}{4} + \epsilon_4 \left[ \frac{15}{4} \cos(\theta)^4 + \frac{3}{8} [1 - \cos(4 \phi)] [-1 + 5 \cos(2 \theta)] + \frac{15}{16} [3 + \cos(4 \phi)] \sin(\theta)^4 \right. \\
&\quad \left. - \frac{9}{4} \left( 1 + \frac{1}{4} [3 + \cos(4 \phi)] \right) \sin(2 \theta)^2 \right] + \epsilon_6 \left( \frac{5}{8} \cos(\theta)^4 [-23 + 37 \cos(2 \theta)] \right. \\
&\quad \left. + \frac{15}{16} [7 + 17 \cos(2 \theta)] \sin(2 \phi)^2 \sin(\theta)^2 - \frac{5}{64} [5 + 3 \cos(4 \phi)] [23 + 37 \cos(2 \theta)] \sin(\theta)^4 \right), \\
e_{13} &= \frac{1}{8} \cos(\theta) \{ 2 \epsilon_4 [-7 + 11 \cos(2 \theta)] + 15 \epsilon_6 [-1 + 9 \cos(2 \theta)] \sin(\theta)^2 \} \sin(4 \phi),
\end{aligned}$$

$$\begin{aligned}
e_{04} = & -\frac{1}{8} + \epsilon_4 \left[ \frac{15}{8} \cos(\theta)^4 + \sin(\theta)^4 + \frac{1}{4} [3 + \cos(4\phi)] \left( \cos(\theta)^4 + \frac{15}{8} \sin(\theta)^4 \right) - \frac{9}{4} \left( 1 + \frac{1}{4} [3 + \cos(4\phi)] \right) \sin(2\theta)^2 \right] \\
& + \epsilon_6 \left\{ \frac{35}{8} \cos(\theta)^6 + \left( -\frac{75}{8} \cos(\theta)^2 + \frac{15}{4} \sin(\theta)^2 \right) \sin(2\theta)^2 \right. \\
& \left. + \frac{1}{8} [5 + 3 \cos(4\phi)] \left[ \frac{35}{8} \sin(\theta)^6 + \left( \frac{15}{4} \cos(\theta)^2 - \frac{75}{8} \sin(\theta)^2 \right) \sin(2\theta)^2 \right] \right\}.
\end{aligned}$$

- 
- [1] A.A. Chernov, *J. Cryst. Growth* **24/25**, 11 (1974).
- [2] P. Nozieres, in *Solids Far from Equilibrium*, edited by C. Godreche (Cambridge University Press, London, 1992), pp. 1–154.
- [3] R.F. Sekerka, *J. Cryst. Growth* **128**, 1 (1993).
- [4] C. Herring, in *The Physics of Powder Metallurgy*, edited by W.E. Kingston (McGraw-Hill, New York, 1951); in *Structure and Properties of Solid Surfaces*, edited by C.S. Smith and R. Gomer (University of Chicago Press, Chicago, 1953), pp. 5–81.
- [5] W.W. Mullins, *Metal Surfaces* (Am. Soc. for Metals, Metals Park, OH, 1963), pp. 17–66.
- [6] N. Cabrera, *Symposium on Properties of Surfaces* (American Society for Testing and Materials, Philadelphia, 1963), pp. 24–31.
- [7] J.W. Cahn and D.W. Hoffman, *Acta Metall.* **22**, 1205 (1974).
- [8] J. Stewart and N. Goldenfeld, *Phys. Rev. A* **46**, 6505 (1992).
- [9] F. Liu and H. Metiu, *Phys. Rev. B* **48**, 5808 (1993).
- [10] J.E. Taylor and J.W. Cahn, *Physica D* **112**, 381 (1998).
- [11] D. Knoppik and A. Löscher, *J. Cryst. Growth* **34**, 332 (1976).
- [12] T.E. Madey, J. Guan, C.-H. Nien, C.-Z. Dong, H.-S. Tao, and R.A. Campbell, *Surf. Rev. Lett.* **3**, 1315 (1996).
- [13] C.-H. Nien and T.E. Madey, *Surf. Sci.* **380**, L527 (1997).
- [14] J.W. Cahn and J.E. Hilliard, *J. Chem. Phys.* **28**, 258 (1958).
- [15] W.W. Mullins, *Philos. Mag.* **6**, 1313 (1961).
- [16] M.E. Gurtin, *Thermomechanics of Evolving Phase Boundaries in the Plane* (Clarendon Press, Oxford, 1993).
- [17] A.A. Golovin, S.H. Davis, and A.A. Nepomnyashchy, *Physica D* **122**, 202 (1998).
- [18] Y. Saito and M. Uwaha, *J. Phys. Soc. Jpn.* **65**, 3576 (1996).
- [19] K. Leung, *J. Stat. Phys.* **61**, 345 (1990).
- [20] C.L. Emmott and A.J. Bray, *Phys. Rev. E* **54**, 4568 (1996).
- [21] J. Krug, *Adv. Phys.* **46**, 139 (1997).
- [22] S.R. Coriell and R.F. Sekerka, *J. Cryst. Growth* **34**, 157 (1976).
- [23] M.J. Kelley, *Scr. Metall. Mater.* **33**, 1493 (1995).
- [24] G.B. McFadden, S.R. Coriell, and R.F. Sekerka, *J. Cryst. Growth* **91**, 180 (1988).
- [25] A.A. Golovin and S.H. Davis, *Physica D* **116**, 363 (1998).
- [26] D.E. Wolf, *Phys. Rev. Lett.* **67**, 1783 (1991).
- [27] A.-L. Barabasi, M. Araujo, and H.E. Stanley, *Phys. Rev. Lett.* **68**, 3729 (1992).
- [28] H.C. Fogedby, *Phys. Rev. E* **57**, 2331 (1998).
- [29] M. Uwaha, *J. Cryst. Growth* **80**, 84 (1987).
- [30] E. Yokoyama and R.F. Sekerka, *J. Cryst. Growth* **125**, 389 (1992).
- [31] M. Siegert and M. Plishke, *Phys. Rev. Lett.* **73**, 1517 (1994).
- [32] P.W. Bates, P.C. Fife, R.A. Gardner, and C.K.R.T. Jones, *Physica D* **104**, 1 (1997).
- [33] A.R. Umantsev, *Sov. Phys. Crystallogr.* **30**, 87 (1985).
- [34] D.J. Wollkind, in *Preparation and Properties of Solid State Materials*, edited by W. R. Wilcox (Dekker, New York, 1979), Vol. 4, pp. 111–191.
- [35] A.R. Umantsev and A.L. Roitburd, *Sov. Phys. Solid State* **30**, 651 (1988).
- [36] D.C. Sarocka and A.J. Bernoff, *Physica D* **85**, 348 (1995).
- [37] J. Bloem, Y.S. Oei, H.H.C. de Moor, J.H.L. Hanssen, and L.J. Giling, *J. Cryst. Growth* **65**, 399 (1983).
- [38] E. Bauser and K.S. Löchner, *J. Cryst. Growth* **55**, 457 (1981).
- [39] J.E. Van Nostrand, S.J. Chey, M.-A. Hasan, D.G. Cahill, and J.E. Greene, *Phys. Rev. Lett.* **74**, 1127 (1995).
- [40] J.E. Van Nostrand, S.J. Chey, and D.G. Cahill, *J. Vac. Sci. Technol. B* **13**, 1816 (1995).
- [41] E. B. Dussan V, *Ann. Rev. Fluid Mech.* **11**, 371 (1979).
- [42] P.G. de Gennes, *Rev. Mod. Phys.* **57**, 827 (1985).
- [43] H.-J. Ernst, F. Fabre, R. Folkerts, and J. Lapujoulade, *Phys. Rev. Lett.* **72**, 112 (1994).
- [44] R. Toral, A. Chakrabarti, and J.D. Gunton, *Physica A* **213**, 41 (1995).
- [45] J.-I. Nishizawa, T. Terasaki, and M. Shimbo, *J. Cryst. Growth* **17**, 241 (1972).
- [46] M.K. Mazumder, Y. Mashiko, M.H. Koyama, Y. Takakuwa, and N. Miyamoto, *J. Cryst. Growth* **155**, 183 (1995).
- [47] T. Hibiya, H. Suzuki, I. Yonenaga, S. Kimura, T. Kawaguchi, T. Shishido, and T. Fukuda, *J. Cryst. Growth* **144**, 213 (1994).
- [48] D. Jacob, Y. Androussi, T. Benabbas, P. Francois, D. Ferre, A. Lefebvre, M. Gendry, and Y. Robach, *J. Cryst. Growth* **179**, 331 (1997).
- [49] J.R. Heffelfinger and C.B. Carter, *Surf. Sci.* **389**, 188 (1997).
- [50] C. Orme, M.D. Johnson, K.-T. Leung, B.G. Orr, P. Smilauer, and D. Vvedensky, *J. Cryst. Growth* **150**, 128 (1995).
- [51] A.J. Bray, *Adv. Phys.* **43**, 357 (1994).
- [52] S. Song, M. Yoon, S.G.J. Mochrie, G.B. Stephenson, and S.T. Milner, *Surf. Sci.* **372**, 37 (1997).
- [53] M. Yoon, S.G.J. Mochrie, M.W. Tate, S.M. Gruner, and E.F. Eikenberry, *Phys. Rev. Lett.* **80**, 337 (1998).
- [54] W. Van Erk, H.J.G.J. Van Hoek-Martens, and G. Bartels, *J. Cryst. Growth* **48**, 621 (1980).
- [55] H. Bethge and K.W. Keller, *J. Cryst. Growth* **23**, 105 (1974).
- [56] B. Lampert and K. Reichelt, *J. Cryst. Growth* **51**, 203 (1981).
- [57] T. Surek, J.P. Hirth, and G.M. Pound, *J. Cryst. Growth* **18**, 20 (1973).
- [58] A.J. Bernoff and A.L. Bertozzi, *Physica D* **85**, 375 (1995).